AD-A175 912 BLUE-GREEN LASER DIODE RESEARCH PROGRAM(U) MINNESOTA MINING AND MFG CO ST PAUL ELECTRONIC AND INFORMATION SECTOR LAB OCT 86 N00014-85-C-0552 1/1

UNCLASSIFIED F/G 20/5 NL

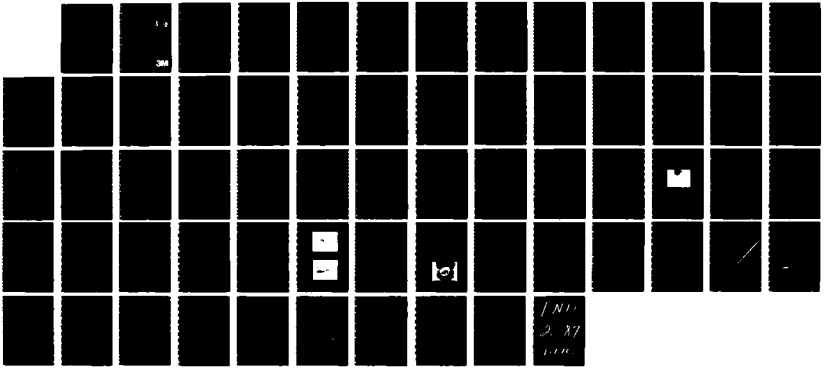

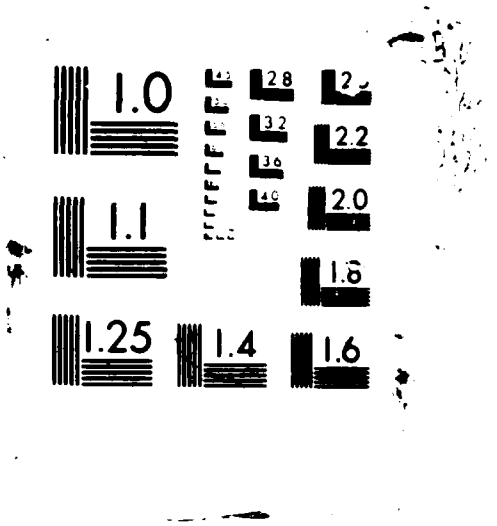
1.0
1.1
1.25
1.4
1.6
2.0
2.2

BLUE-GREEN LASER DIODE RESEARCH PROGRAM

Quarterly Technical Progress Report No. 2
For The Period July 1, 1986 To September 30, 1986

Prepared Under
Contract Number N00014-85-C-0552

OCTOBER, 1986

The views and conclusions contained in this document are those of the authors and should not be interpreted as necessarily representing the official policies, either expressed or implied, of the Defense Advanced Research Projects Agency or the U.S. Government.

Work supported in part by the:

DEFENSE ADVANCED RESEARCH PROJECTS AGENCY
1400 Wilson Boulevard
Arlington, VA 22209

Under the:

OFFICE OF NAVAL RESEARCH
Department Of The Navy
800 N. Quincy Street
Arlington, VA 22217-5000

Electronic and Information
Sector Laboratories/3M
St. Paul, MN 55144

3M

EXECUTIVE SUMMARY

Throughout the fourth quarter of the first program year, work in the St. Paul Laboratory has concentrated on completing the "growth matrix" study relating the properties of ZnSe grown on (100) GaAs to growth temperature (T_g) and beam-pressure ratio (BPR). In the same period, the Toronto effort has concentrated on a comparison of the properties of ZnSe films grown on (100) GaAs with those grown on (100) Ge during the same growth run.

In the course of the above efforts, there have been several achievements which are particularily noteworthy in that they indicate that our epitaxial films are of exceptionally high quality. First we have achieved the highest peak mobility (above 7,000 $cm^2/V.$ sec.) ever observed for MBE-grown ZnSe. Second, we have reduced the donor concentration and, thereby, increased the compensation ratio to the point that unintentionally-incorporated acceptor bound exciton emission is clearly discernible in the photoluminescence spectra. Lastly, we have demonstrated, for the first time, electron-beam pumped laser action in epitaxial ZnSe films, and have observed low threshold current densities at temperatures as high as room temperature.

The St. Paul growth matrix study has revealed some general trends in T_g-BPR space which we feel will aid us in the p-doping studies now in progress. In general, donor and electron concentrations tend to decrease, and mobilities increase, as T_g and BPR increase. Thus, growth in the high T_g, high BPR region seems to produce optimized electrical properties. However, in photoluminescence spectra, the highest R value and narrowest donor-bound exciton emission lines are observed near BPR = 1/2:1 and T_g = 300. Thus there may be some trade-offs in optimizing both electrical and optical properties.

This conclusion, however, is tentative for two reasons. First, we have experienced difficulty in electrical measurements on the high resisitivity samples grown at high T_g and high BPR. Attempts to overcome this difficulty are now being made via development of the photo-Hall technique. Second, it is at present unclear just how important R-value is in determining the suitability of ZnSe for opto-electronic devices.

In addition to the above general trends, several significant specific results came from the ZnSe/GaAs effort this quarter. Preliminary studies of the relationship between growth rate and photoluminescence indicate a reduction in film quality for growth rates below approximately 1 μ/hour; this result conflicts with observations in other laboratories which indicate improved quality at lower growth rates. Newly begun selective excitation photoluminescence and resonance Raman studies (the first of their kind for MBE-grown ZnSe) point to Ga and Cl as principal extrinsic donors in our films, and suggest that the I_{2_0} and I_x donor-bound-exciton may be related to the same chemical species. Lastly, SIMS imaging studies (the first of their kind) and voltage offset studies have revealed that specific film defects are responsible for spurious high Ga and Al signals, and have ruled out Al, Ga, and In as the dominant electrically active donors in films with donor concentrations above 10^{16} cm^{-3}.

In the course of the Toronto comparative study, it has been demonstrated that, for films grown on GaAs and Ge to the same thickness with a BPR of 1:1, donor-bound-exciton (DBE) PL linewidths as well as double-crystal x-ray rocking curve (DCRC) linewidths are minimized at a growth temperature of 330°C, independent of the substrate identity. However, it is found that the films on Ge must be grown to a greater thickness before the minimum linewidths are attained, 6.5 μ for Ge as compared to 2 μ for GaAs, and even at 6.5 μ thickness the linewidths for films on Ge substrates are broader than for those on GaAs substrates.

Because of these indications that the structural quality of the ZnSe/Ge is inferior to that of the ZnSe/GaAs, and the difficulties experienced in electrical evaluation of the ZnSe/Ge samples, it has been decided to de-emphasize the Ge substrate effort in favor of doping studies on GaAs substrates.

The principal difficulty that has been encountered to date has been in performing electrical characterization of samples. Irreproducibility of contacts has rendered DLTS useless for the moment. Therefore capacitance spectroscopy is being developed as an alternate means of studying trap states; an in-situ metallization chamber is being added to the MBE system to improve contact reproducibility. The high resistivity of some films, and/or the low resitivity of the Ge substrates, have made reliable Hall measurements impossible for some samples. Photo-Hall and substrate removal techniques are currently being developed to address these problems.

In the next program quarter, program emphasis will turn to growth and characterization of p-doped samples. Initial studies in St. Paul will employ sodium as the acceptor dopant; those in Toronto will employ nitrogen.

TABLE OF CONTENTS

LIST OF FIGURES

LIST OF FIGURES (continued)

Figure **Page**

LIST OF TABLES

1.0 INTRODUCTION

This report covers progress during the tenth through twelfth months of ONR Contract N00014-85-C-0552. The various sections of the report are numbered and titled using the format of the original proposal. As before, results from parallel programs at 3M-St. Paul and 3M-Toronto are discussed.

2.0 PROGRESS REPORT

2.1 Project I, Task 1: Materials Research - Undoped ZnSe Research

2.1.1 ZnSe Heteroepitaxy On (100) GaAs

During the past three months (July 1 to September 30), fourteen unintentionally doped ZnSe layers (ZSE47 to ZSE60) were grown on GaAs substrates (N^+ and semi-insulating), despite several setbacks experienced in the MBE system. These growth runs, together with some runs in the previous three-month period, complete the 4 x 4 growth parameter matrix study. A very clear trend can be found in structural, electrical, and optical properties of these films grown under different growth conditions. So far, the lowest room temperature carrier concentration we get is 5×10^{15} cm^{-3}, and the highest peak mobility is 7200 cm^2/V-sec, which is the best result ever reported in MBE-grown ZnSe layers. Detailed results will be discussed elsewhere in this report.

Some of the specimens were grown at the same substrate temperature, T_g, and beam pressure ratio, BPR, but at different growth rates. The purpose is to understand the influence of growth rate on impurity incorporation, strain relief, and dislocation propagation.

A new 2 cc source oven was installed in the II-VI growth chamber and was outgassed at 1200°C for two hours. This oven is for p-type doping material and will be loaded with Na_2Se at next source replenishment.

2.1.1.1 The Growth Of ZnSe Epitaxial Layers On (100) GaAs

A. Group 1 (ZSE47 to ZSE58) - The surface morphology of the sixteen specimens in the matrix is mostly shiny and smooth except for samples grown at higher BPR (2:1). Overgrowth of yellowish color, possibly ZnSe, can be found on these films. Some of the overgrowth can be blown off with an N_2 gun. Close examination by optical microscopy and surface profiling by Dektak indicates that the overgrowth is probably formed somewhere else in the system and is later deposited on the sample surface during the growth run. Under the present growth conditions, it is likely that these flakes are formed in one of the source ovens and then ejected by the high beam pressure. Efforts have been made to change the shape of the starting

materials but it is unclear whether the overgrowth problem can be thereby resolved. The surface of ZSE57 (T_g = 400 C, BPR = 2:1 is very cloudy. This is the only cloudy sample we have seen so far. We believe that the effective BPR is greater than 2:1, due to the higher growth temperature.

B. Group 2 (ZSE59 to ZSE60) - The growth rate of our samples has been about 0.7 to 1.2 μ/hour. We have been told by persons in other labs that they are not able to grow ZnSe films with good quality if the growth rate is higher than 0.5 μ/hour. In order to explore whether we can further improve the properties of our films by reducing the growth rate, we decided to grow sets with the same substrate temperature and beam pressure ratio, but different absolute beam pressures and thus different growth rates. Initial experiments with T_g = 350°C, 1:1 BPR, and growth rates of 0.3 and 0.5 microns/hour indicated a degradation in photoluminescence properties at the lower growth rates. However, a high growth rate sample grown in this series showed somewhat degraded PL also. Therefore, the results of the growth rate study are now being checked, this time with T_g = 350°C and BPR = 1/2:1. The intended growth rate will be 0.5 1.0 μ/hour. The growth time for each sample will be adjusted in such a way that film thicknesses will be the same. These specimens will be characterized by double crystal x-ray diffraction, XTEM, Hall, and photoluminescence.

2.1.1.2 Photoluminescence And Raman Scattering Measurements On ZnSe/(100) GaAs

Routine PL measurements were made on the remaining samples in the T_g/BPR growth matrix study (#ZSE47A-ZSE58A). In general, we find the relevant PL properties [donor-bound exciton intensity and linewidth, and the R-value, i.e., the ratio of near-band edge emission (NBE) to deep-level (DL) emission intensities] deteriorate as we get to the extremes of the growth parameter space. Figure 2-1 is the PL spectrum obtained for such a sample (#ZSE46A, T_g = 400°C, BPR = 1/4:1). The NBE emission is weak, with broad DBE peaks, and the R-value has diminished to approximately 8, compared with a typical value of 1000 for a sample grown nearer the center of the growth parameter space. Table 2-1 summarizes the PL properties for all the samples in this study and should be compared with Table 2-2 which summarizes the corresponding electrical properties. The spectrum of one of these samples is worthy of special notice. In Figure 2-2 we show the 9K PL spectrum for sample ZSE56A (T_g = 300°C, BPR = 2:1.)

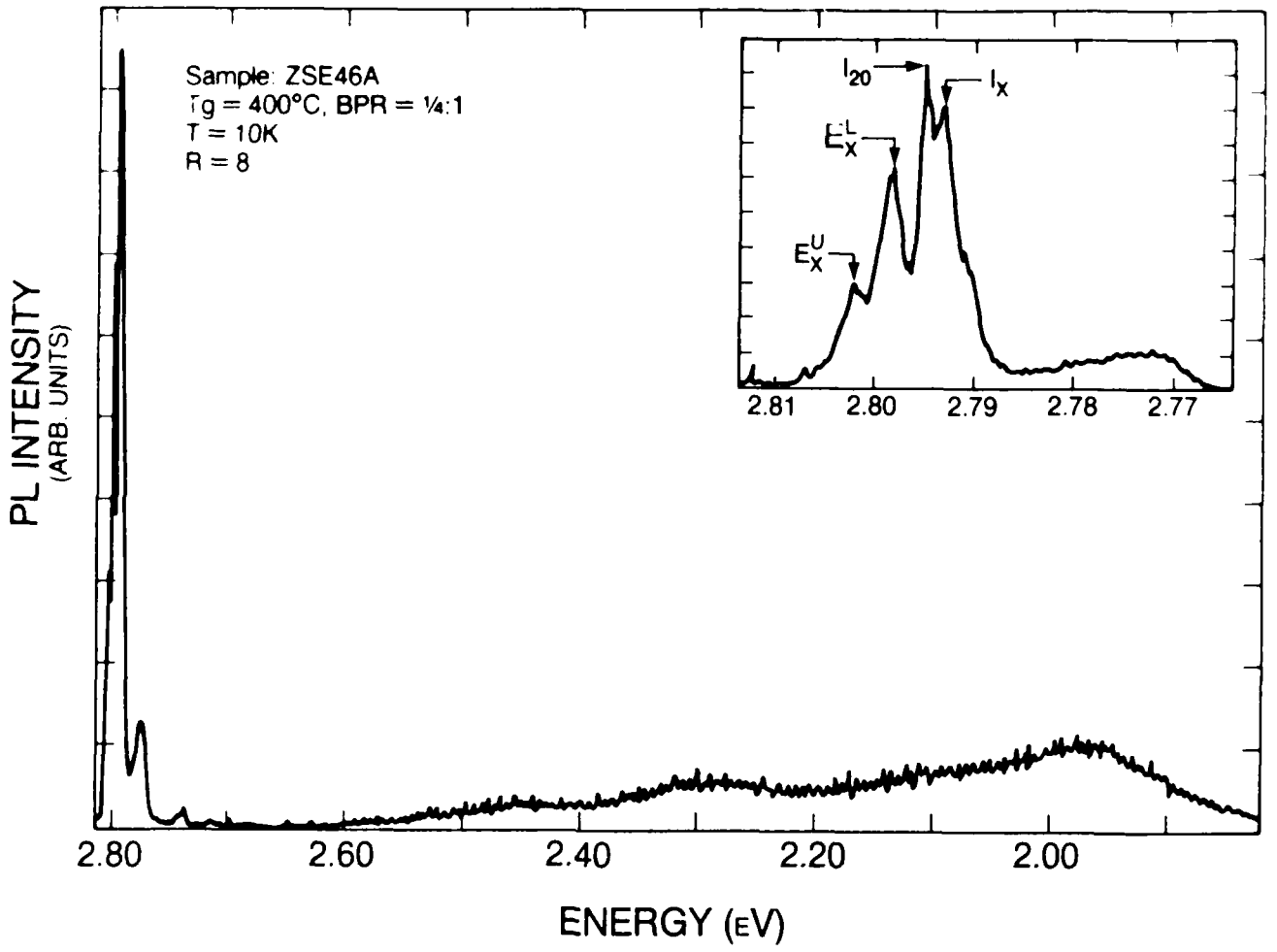

Figure 2-1. Low Temperature Photoluminescence Spectrum For A Sample Grown Under Conditions Near The Edge Of The Growth Parameter Space Covered In This Study. The Near-Band-Edge Emission Is Relatively Weak And The R-Value Is Among The Smallest Measured.

TABLE 2-1. Summary Of Optical Measurements On Samples Grown In T_g - BPR Growth Matrix Study. R = Int(NBE)/Int(DL), I_x Is The Intensity Of The (Unidentified) Donor-Bound Exciton Peak I_x, ΔE Is The Linewidth Of I_x.

BPR \ T_g	250	300	350	400
1/4:1	R = 400 $I_x = 1.5 \times 10^4$ $\Delta E = 3.75$* DAP 2.6937 *I_2, I_x folded 51 50	R = 400 $I_x = 2.0 \times 10^4$ $\Delta E = 2.4$ 47 shows Y^o & SAL 49	R = 300 $I_x = 3.7 \times 10^4$ $\Delta E = 2.5$ SAL DL Some M 45	R = 8 $I_x = 1500$ $\Delta E = 3.75$ $I_{20} > I_x$ Cu-red DL Some I_1 46
1/2:1	R = 1030 $I_x = 1.1 \times 10^5$ $\Delta E = 3.38$* DAP 2.7339 *I_2, I_x folded 52	R = 1100 $I_x = 2.0 \times 10^5$ $\Delta E = 2.25$ 43	R = 700 $I_x = 1.0 \times 10^5$ $\Delta E = 2.0$ 42 36 48	R = 40 $I_x = 2.0 \times 10^4$ $\Delta E = 2.0$ Some M SAL DL Strong I, D 39
1:1	R = 29 $I_x = 3.6 \times 10^4$ $\Delta E = 3.75$ Some M SAL DL 41	R = 500 $I_x = 1.0 \times 10^5$ $\Delta E = 2.0$ 40	R = 830 $I_x = 1.0 \times 10^5$ $\Delta E = 1.6$ Some M 37	R = 13 $I_x = 7500$ $\Delta E = 2.5$ Cu-grn.DL $\Delta(I_{20}) \simeq 1$ meV Some I DAP 38 44
2:1	R = 660 $I_x = 7.73 \times 10^3$ $\Delta E = 2.25$ Some M, DAP SAL DL 58	R = 150 $I_x = 3.6 \times 10^3$ $\Delta E = 3.0$ I_1? at 2.7918 with DAP $I_1 > I_2$ 56	R = 40 $I_x = 8.0 \times 10^3$ $\Delta E = 2.0$ Cu-grn DL $I_1^D = .15\ I_x$ I(2.791) $\simeq .15\ I_x$ 55 53	R = 0.2 $I_x = 2.0 \times 10^2$ $\Delta E = 2.25$ Cu-grn dominate $I_{20} > I_x$ $I_1^D \simeq I_{2,10}$ $I_1^D \simeq I_{2,10}$ Some I_1 57

TABLE 2.2. Summary Of The Electrical Measurement Made On ZnSe/GaAs Samples Grown At Various Growth Temperatures, T_g, and Zinc: Selenium Beam Pressure Ratios, BPR. Given Are The Peak Mobility, μ_p, The Room Temperature Carrier Concentration, n_{300}, And The Calculated Donor And Acceptor Concentrations, N_D And N_A.

T_g / BPR	250	300	350	400
1/4:1	μ_p = 1142 N_D = 1.2 x 10^{17} N_A = 1.1 x 10^{15} n_{300} = 9.9 x 10^{16} ZSE51A ZSE50A	μ_p = 1191 N_D = 9.5 x 10^{16} N_A = 9.0 x 10^{14} n_{300} = 8.1 x 10^{16} ZSE49A ZSE47A	μ_p = 2303 N_D = 9.8 x 10^{16} N_A = 7.3 x 10^{16} n_{300} = 2.1 x 10^{16} ZSE45A	measured with C_V $n_{300} \leq 5 \times 10^{15}$ ZSE46A
1/2:1	μ_p = 1567 N_D = 1.5 x 10^{17} N_A = 7.2 x 10^{16} n_{300} = 6.37 x 10^{16} ZSE52A	μ_p = 2132 N_D = 1.7 x 10^{17} N_A = 1.1 x 10^{17} n_{300} = 4.9 x 10^{16} ZSE43A	μ_p = 3724 N_D = 5.8 x 10^{16} N_A = 4.2 x 10^{16} n_{300} = 1.5 x 10^{16} ZSE42A ZSE36A ZSE48A	μ_p = 3900 measured in room light n_{300} = 1.1 x 10^{15} μ_{300} = 280 ZSE39A
1:1	μ_p = 1476 N_D = 9.5 x 10^{16} N_A = 8.0 x 10^{16} n_{300} = 1.4 x 10^{16} ZSE41A	μ_p = 2403 N_D = 8.2 x 10^{16} N_A = 3.7 x 10^{16} n_{300} = 4.0 x 10^{16} ZSE40A	μ_p = 5638 N_D = 3.3 x 10^{16} N_A = 2.3 x 10^{16} n_{300} = 9.4 x 10^{15} ZSE37A	μ_p = 2040 measured in room light n_{300} = 3.2 x 10^{14} μ_{300} = 320 ZSE44A ZSE38A
2:1	μ_p = 3059 N_D = 5.8 x 10^{16} N_A = 3.8 x 10^{16} n_{300} = 1.9 x 10^{16} ZSE58A	μ_p = 7148 N_D = 2.5 x 10^{16} N_A = 1.9 x 10^{16} n_{300} = 5.6 x 10^{15} ZSE56A	measured in room light μ_{300} = 333 n_{300} = 3.07 x 10^{14} ZSE55A ZSE53A	measured in room light μ_{300} = 290 n_{300} = 3 x 10^{12} ZSE57A

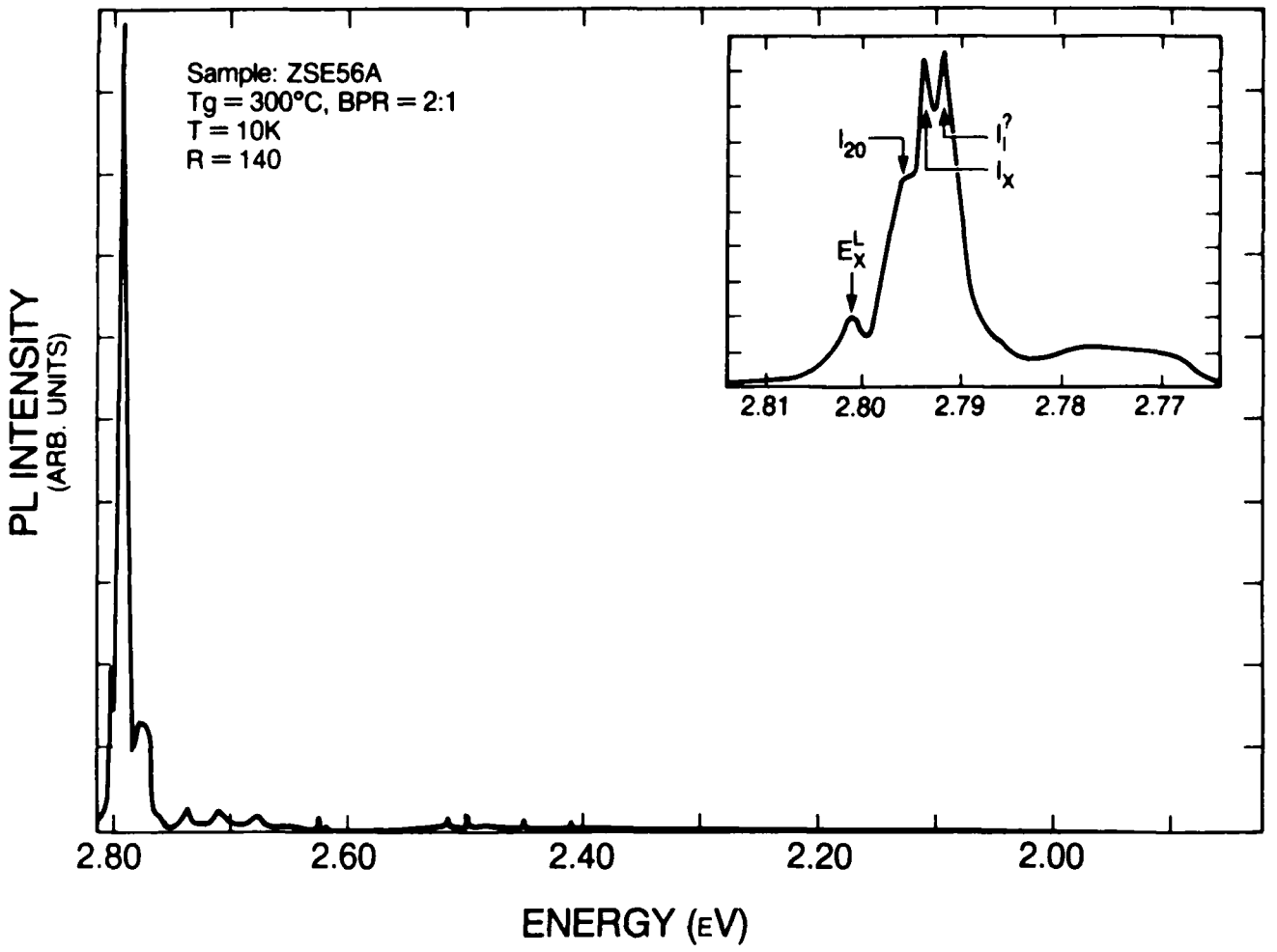

Figure 2-2. Low Temperature Photoluminescence Spectrum For Sample #ZSE56A In Which We Observe, For The First Time, Dominant Near-Band-Edge Emission From An Acceptor-Bound-Exciton Peak.

This spectrum is dominated by a peak at 2.7918 eV, which lies below the positions of I_x and I_{20}, in the region where one would expect acceptor-bound exciton emission (A°, X).

Assuming that this peak does originate from an acceptor, we calculate its binding energy to be approximately 95 meV (of the known acceptors, only N and Li have BE's this small). This sample also shows some emission in the DA pair region, and the acceptor binding energy calculated from the position of the zero-phonon DAP peak also lies in the vicinity of 100 meV. There is little evidence for this peak in the spectra of other samples. Interestingly enough, this sample also shows the highest peak mobility we (or anyone) have observed to date (> 7100 cm^2/V_s.) It also shows the lowest N_D and one of the highest compensation ratios and lowest n_{300} values observed in our growth matrix.

We also measured the PL for two films in the growth rate study: ZSE59A (BPR = 1/2:1/2) and ZSE60A (1/4:1/4). These films show much poorer PL spectra (weaker and broader DBE emission, low R-values, and emission from defect-related bands) than the 1:1 counterparts grown earlier in the study.

We have devoted further attention to the Raman scattering spectra for sample ZSE20A (t = 0.23 μ) where we have seen some peculiar scattering features in the vicinity of the ZnSe and GaAs optic phonon regions (Figure 2-3). We intend to repeat these measurements using a Kr laser which is resonant with an electronic transition in GaAs (our earlier measurements were done near resonance with the fundamental gap in ZnSe and clearly show a resonance behavior--no scattering was seen near the 223, 250 and 290 cm^{-1} regions when the 5145A line was used for excitation). We believe that the observed scattering features can be accounted for by scattering from phonons bound to the interfaces. Using the condition [1]

$$\varepsilon_1(\omega) = \varepsilon_2(\omega)$$

$$\varepsilon i(\omega) = \varepsilon_\infty \left[\frac{\omega^2 - \omega_{lo,\,i}}{\omega^2 - \omega_{TO,\,i}} \right]$$

where $\varepsilon_i(\omega)$ is the dielectric function for medium i, we calculate that at the GaAs/ZnSe interface, there should be solutions at 221.2 and 289.9 cm^{-1}, while at the ZnSe/air interface there should be a single solution at 250.1 cm^{-1}, in excellent agreement with the observed results. A plot of the dielectric functions for the three media is shown in Figure 2-4.

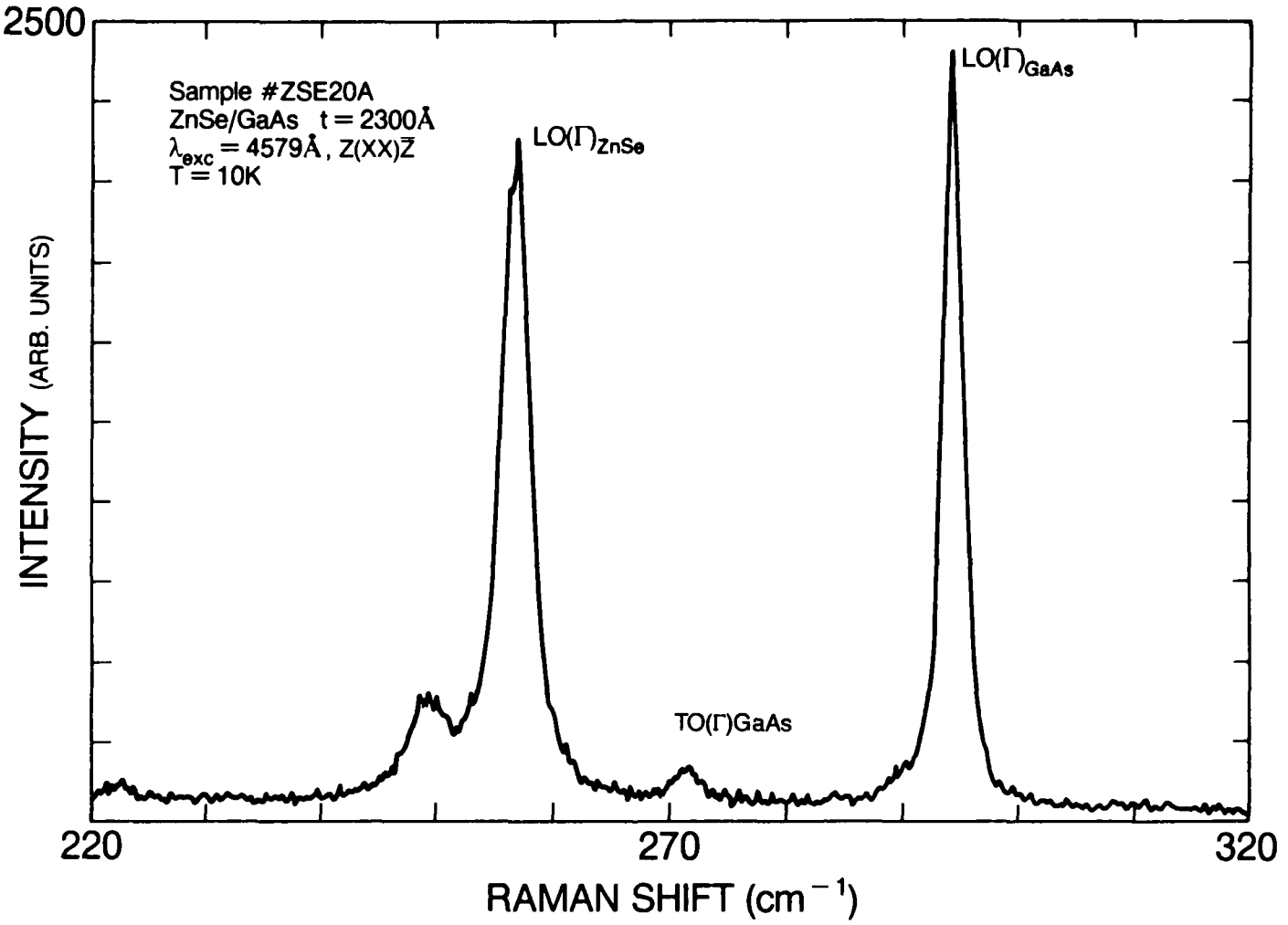

Figure 2-3. Low Temperature Raman Scattering Spectrum From A Thin (0.23 μ) Film Of ZnSe On (100) GaAs. The Exciting Laser Line Is At 4579A, Near An Excitonic Resonance For The ZnSe. The LO Phonon Peaks For ZnSe And GaAs Are Visible Near 256 And 294 cm^{-1}, Respectively. The Peak Near 271 cm^{-1} Is The (Forbidden) TO Peak For GaAs. The Additional Features At 222.8, 249.6, And 290.4 cm^{-1} Are Observed Only Under Resonance Conditions. Their Origins Are Discussed In The Text.

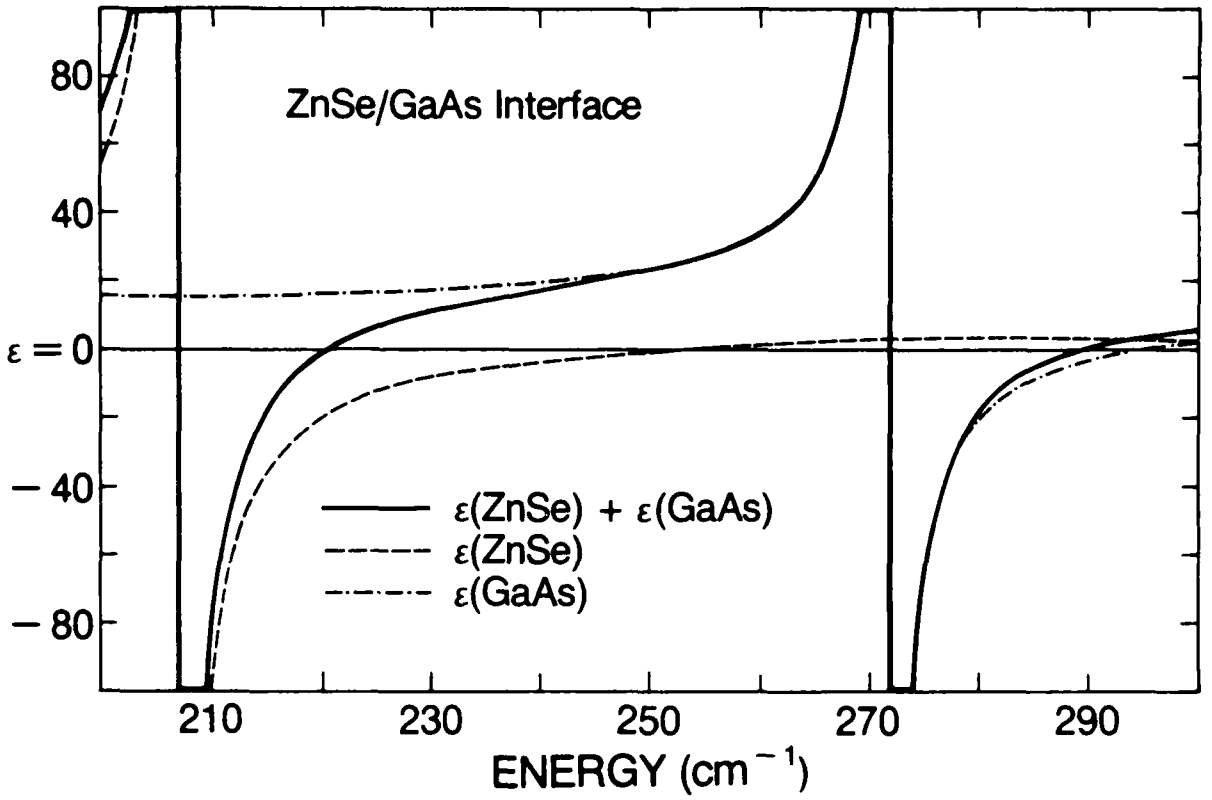

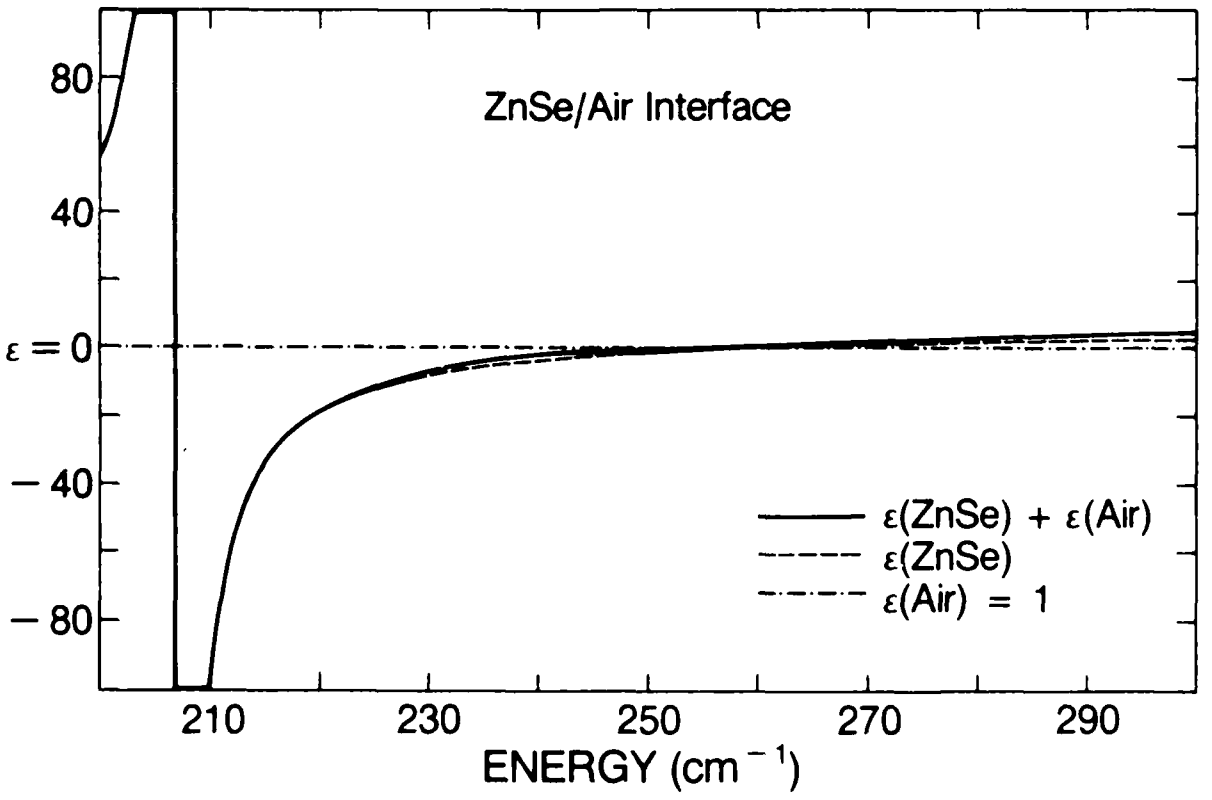

Figure 2-4. The Calculated Dielectric Functions For GaAs, ZnSe, and Air. The Interface Modes Occur When $\varepsilon_1(\omega) + \varepsilon_2(\omega) = 0$.

Currently, we are trying to explain why we are able to observe these modes in this thin sample but not in a 1-2 μ thick film.

It would appear that either: (a) the scattering is induced by the presence of impurities and/or defects near the ZnSe/GaAs interface (accessible because the film is thin), or (b) the incident light is able to reflect off the interface, thereby giving us forward scattering. The resonance behavior seems to be pointing us toward the first of these possibilities.

With the recent acquisition of an Ar-ion-pumped dye laser operating in the near-UV spectral region, we have begun some careful and extensive selective excitation PL (SPL) measurements on sample ZSE25A. This sample was chosen for this study because it has a very well-defined contrast between the I_{2O} and I_x peaks. Figure 2-5 is representative of the type of spectra observed. To the left is shown the conventional PL spectrum of the sample, obtained using above-bandgap incident radiation. In it can be distinguished the upper (E_x^U) and lower (E_x^L) branch polaritons at 2.8027 and 2.7993 eV, and what are believed to be donor-bound exciton peaks I_{2O} (2.7966 eV) and I_x (2.7945 eV.) On the right-hand side of the figure are shown the spectra obtained by exciting the PL with a dye laser tuned through a range of wavelengths in the donor-bound exciton region. The wavelength region scanned is that in which the two-electron donor satellites (TEDS) appear. A number of these TEDS are observed here, their peak intensities (and sometimes their energetic positions) changing rapidly with the exciting wavelength. We can measure with high precision the shift of the TEDS from its parent satellite (i.e., the 1S --> nS or 1S --> nP splitting) which permits a far better identification of the parent donor species than does the 1S position itself, since this latter quantity is strongly influenced by strain, local field fluctuations and near-neighbor bonding arrangements (central cell effects.) In Figure 2-6 we plot the intensity variations observed for three of these TEDS for which the measured displacements from the exciting line are 19.75, 20.5 and 18.5 meV (features labeled A, B, and C, respectively). Feature B is clearly resonant with the line I_{2O} in the NBE emission; its shift (20.5 meV) is very close to that expected for Ga donors [2]. On this basis, we identify I_{2O} as being attributable to Ga, in agreement with many other researchers. Peak B (19.75 meV) exhibits a maximum of intensity near the small DBE peak at 2.7958 eV, although this excitation spectrum may be severely distorted because of strong self-absorption effects near 2.7966 eV.

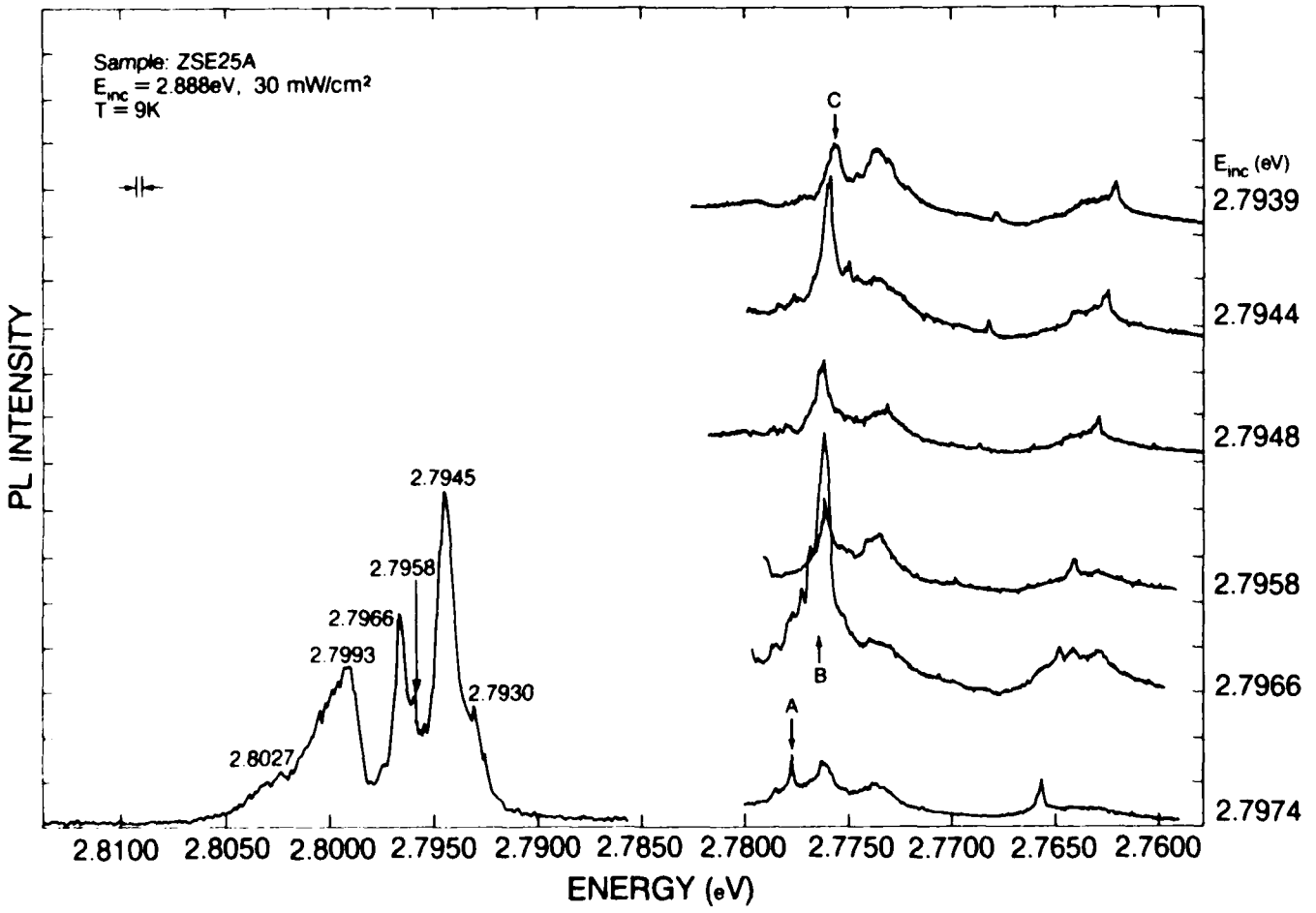

Figure 2-5. Selective Excitation Photoluminescence Spectra For Sample #ZSE25A. On The Left Is Shown The Conventional PL Spectrum For The DBE Region Obtained Using Above-Bandgap Laser Excitation. On The Right Are The Spectra In The Two-Electron Transition Region Obtained Using Laser Excitation Energies In The DBE Region At The Wavelengths Indicated. A PL Feature Appears Unshifted On This Plot As The Excitation Energy Is Varied. The LO-Phonon Raman Scattering Peak Can Be Seen Near 2.765 eV; This Peak Shifts With The Excitation Energy And Can Be Used As A Wavelength Marker.

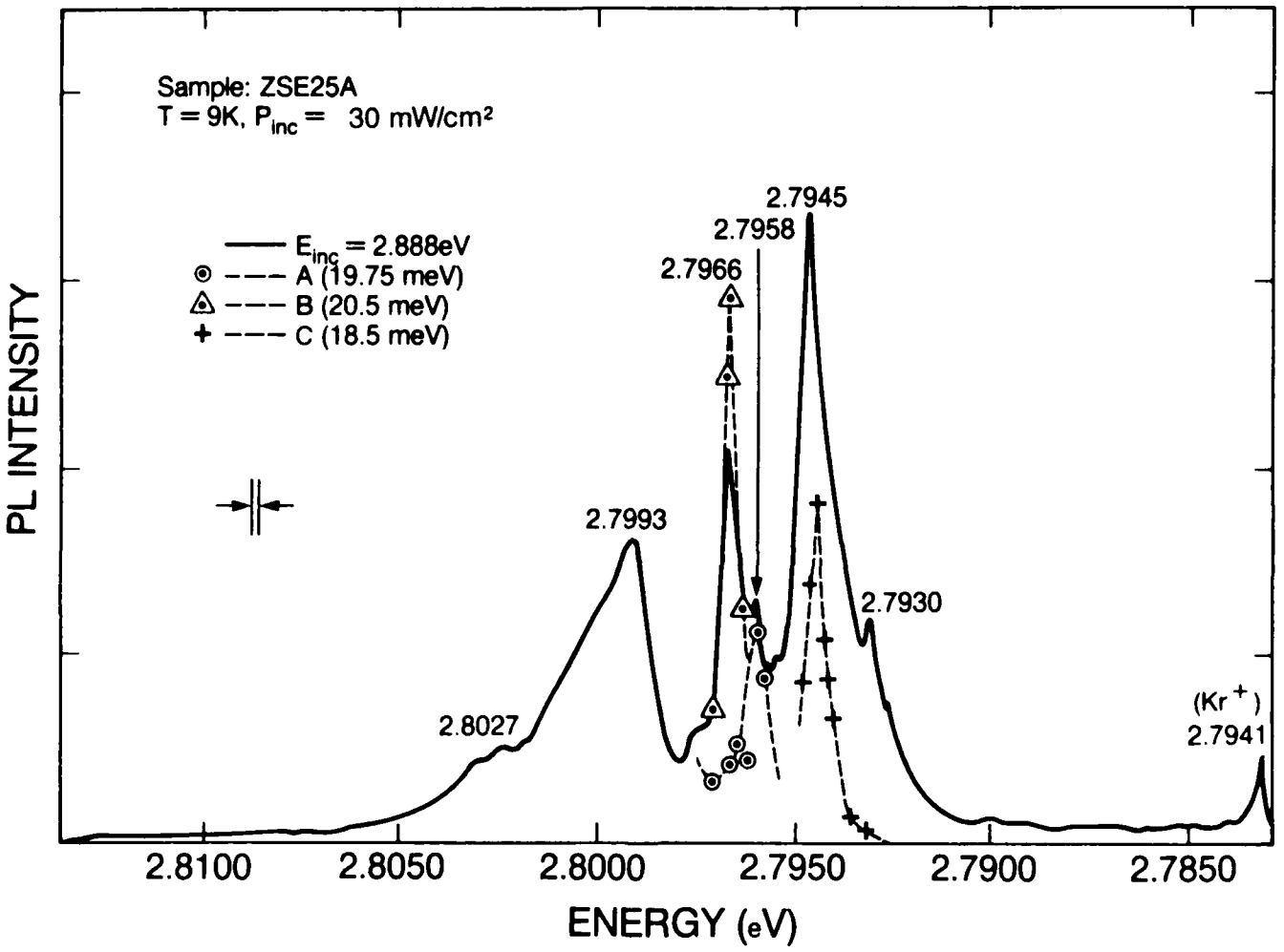

Figure 2-6. Excitation Spectra For Three Of The Features Observed In The SPL Scans Of Figure 2-5. The Solid Line Is The Conventional PL Spectrum For This Sample (Right-Hand Side Of Figure 2-5). The Points Represent The Intensities Of The Respective TEDS Observed Under Excitation At That Wavelength.

On the basis of its 1S --> 2S,P shift, it would appear to be due to Cl donors (E(1S) - E(2S) = 19.3 meV and E(1S) - E(2P) = 19.6 meV according to ref. [2]). Experiments to detect Cl using SIMS are now underway. The third peak, C, is the most interesting. Its shift, 18.5 meV, would indicate that it is associated with a shallow donor, since the donor binding energy is found to grow linearly with the size of the central cell correction, E(2P)-E(1S) [3]. On the other hand, its excitation spectrum indicates that it is associated with I_x which, if it is a neutral donor-bound exciton, must be very strongly bound (E_D > 40 meV according to its 1S position and using Haynes' rule). We are considering a number of possible explanations for this behavior, among them:

a. I_x may be an ionized Ga donor-bound exciton emission peak (I_3). Its position in the gap would favor this assignment over that of a neutral DBE. However, it is difficult to account for its intensity being greater than that of I_{2_0} in almost all of our samples, which exhibit a broad range of compensation ratios. I_3 would exhibit no two-electron transitions but there may be some mechanism by which the ionized donor becomes photoneutralized by the exciting beam; the resulting neutral donor would then exhibit a TEDS at the same absolute energy as it would if it had been excited by radiation at 2.7966 eV. It is noteworthy that features B and C both occur at the same absolute energy (22399 cm^{-1}).

b. I_x may be, as has been suggested [4], a low energy component of the Ga neutral DBE split by strain in the epilayer. This postulate contradicts much of what we know about strain in these layers. In addition, the temperature dependence of the intensities of these peaks is not that which would be predicted for such a strain split pair [ref. Six Month Technical Progress Report No. 1].

c. I_x may be a peculiar type of donor (e.g. V_{Se}) which appears strongly bound and yet, perhaps because of some non-central component to its potential, yields a 1S--2P splitting which is considerably smaller than that for a conventional substitutional donor. The appearance of its 2P TEDS at exactly the same energy as that of the Ga NDBE would then have to be a somewhat remarkable coincidence.

Further experimental and theoretical work is underway to unravel this puzzle.

We have also made measurements of the Resonant Raman scattering (RRS) spectra from sample ZSE25A. By placing the excitation line in the vicinity of the n = 2 exciton and observing the RS which falls in the DBE region, one gets resonant enhancement in both the ingoing and outgoing photon channels, leading to very large RS signals [5]. In Figure 2-7 we show the results of these measurements. In this plot, a Raman signal would be independent of the excitation energy (see the ZnSe LO-phonon signal at 256 cm^{-1}), while a PL signal would shift to higher energies (smaller Raman shift). There is a Raman signal at 156 cm^{-1} which is clearly enhanced as it passes through I_x and, to a lesser extent, through I_{20}. If, as was the case in the reference cited here, this scattering corresponds to a 1S --> 2S transition on a donor site, then the donor in this case would have a 1S --> 2S energy of 19.5 meV which is closer to Cl (19.3) than to Ga (20.1) or In (20.9). We view these results as interesting, but hardly conclusive. They must be interpreted in light of the SPL results and SIMS measurements.

2.1.1.3 Dependence of Hall Measurements on Growth Conditions

From July 1 through September 30, 1986, the ZnSe/GaAs series (ZSE47A - ZSE60A) was grown. Most of the samples in this series were grown to study the effects of the zinc to selenium Beam Pressure Ratio (BPR) and growth temperature (T_g) on film quality. In this section we describe the results of electrical measurements which were made on these samples.

Table 2-2 summarizes the results of our Hall measurements on ZSE36A - ZSE58A. The sample number is shown at the bottom right corner of each box. If two or more samples were grown under the same growth conditions, then the sample number for each sample grown at this condition appears, but only the results of the uppermost sample are presented. The information presented in this matrix includes the peak mobility (μ_p) in cm^2/volt-sec, the donor concentration (N_D) in cm^{-3}, the acceptor concentration (N_A) in cm^{-3}, and the room temperature carrier concentration (n_{300}) in cm^{-3}. During this study the following observations were made:

a. ZSE56A has a peak mobility of approximately 7150 cm^2/volt-sec., a room temperature carrier concentration of 5.6×10^{15} cm^{-3} and a donor density of only 2.5×10^{16} cm^{-3} .
b. The room temperature carrier concentration tends to decrease with increasing T_g and increasing BPR.

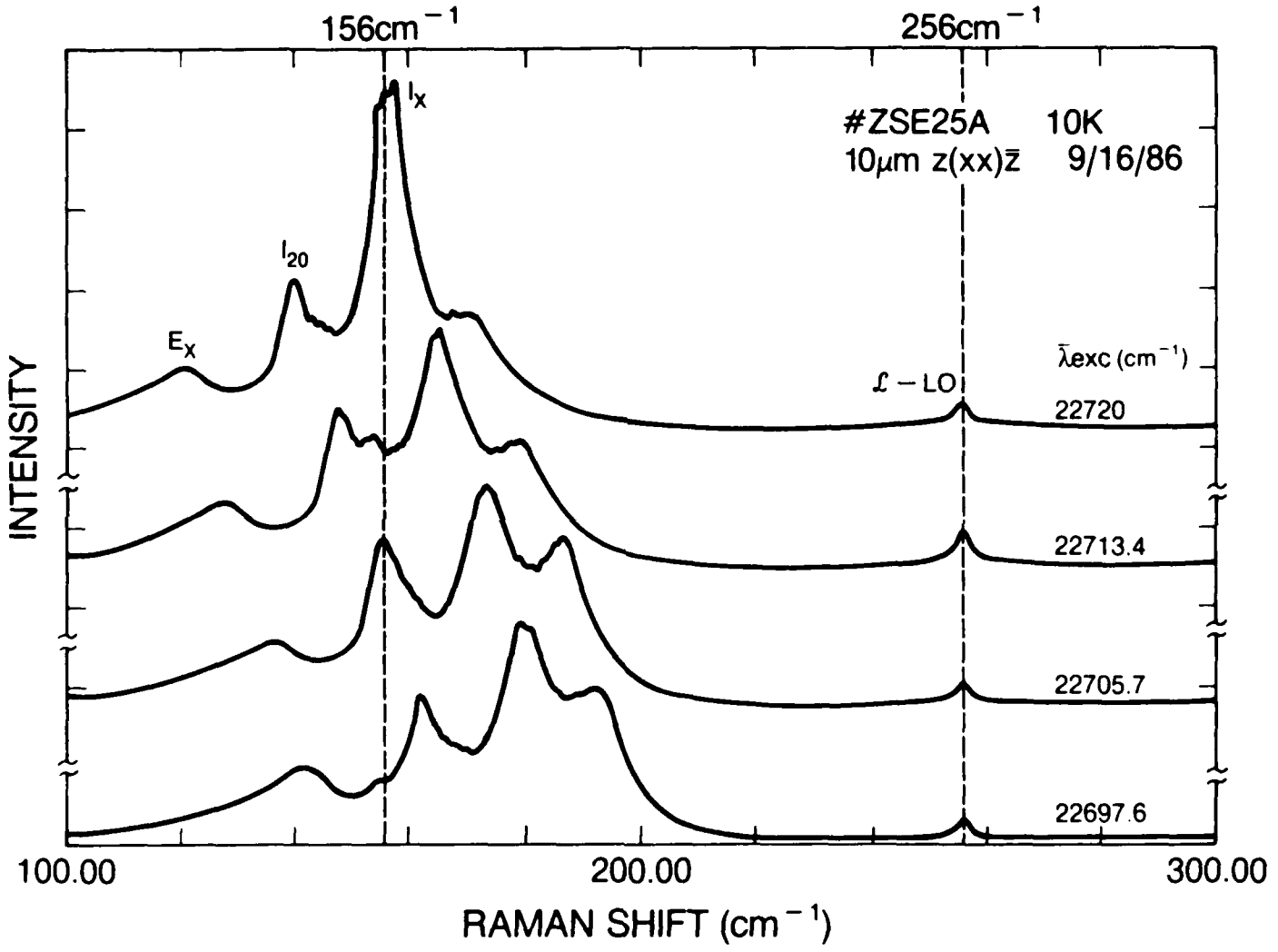

Figure 2-7. Resonance Raman Scattering Spectra For Sample #ZSE25A; The Excitation Wavelengths Are Indicated Alongside Each Curve. A Raman Scattering Feature, Such As The LO Phonon Scattering At 256 cm^{-1}, Appears Unshifted As The Excitation Wavelength Is Varied. The Raman Scattering Feature At 156 cm^{-1} Is Discussed In The Text.

c. The peak mobility tends to increase with increasing BPR.

d. Samples grown at 400°C have large "dark" resistivity and are strongly photoconductive.

ZSE56A is an extraordinary sample. The peak mobility measured in this sample is the largest ever reported for MBE-grown ZnSe. The mobility and carrier concentration measured from ZSE56A as functions of temperature are shown in Figures 2-8 and 2-9. Assuming partial compensation and non-degeneracy, we calculate donor and acceptor concentrations of 2.5×10^{16} and 1.9×10^{16} cm^{-3}, respectively, for this sample. These low values along with the large peak mobility indicate exceptional film quality.

Several plots were made in order to determine which growth condition produced the highest quality films. First the room-temperature carrier concentrations at fixed BPR are plotted as a function of growth temperature in Figure 2-10. From this figure it is seen that n_{300} tends to decrease with increasing T_g. It should be noted that the measurements for samples grown at 400°C were obtained with the sample illuminated by room light or by C-V measurements. We also plotted n_{300} as a function of BPR with the growth temperature fixed (Figure 2-11). In Figure 2-11 it is seen that the room temperature carrier concentration decreases with increasing BPR. Another criterion which must be included when judging the quality of intrinsic semiconducting films is the mobility of the carriers. The peak electron mobility at constant growth temperature is plotted as a function of BPR in Figure 2-12. The peak mobility is seen to increase with increasing BPR for fixed T_g.

Low carrier concentration along with large carrier mobility is requisite of high quality intrinsic semiconductors. From these considerations the present study indicates that the optimum growth conditions are: 1) BPR = 2; 2) T_g = 300°C. These conditions, however, have been determined without a complete understanding of ZSE53A, ZSE55A, and all the samples grown at 400°C. More refined measurements of these samples may result in a revaluation of the optimum growth parameters.

All samples with large dark resistivities have also been found to be very photosensitive. Not only do the carrier concentrations increase when light is incident upon the semiconducting film, but the mobility of the carriers also shows a marked increase. A model which may explain this phenomenon requires the presence of doubly negative sites.

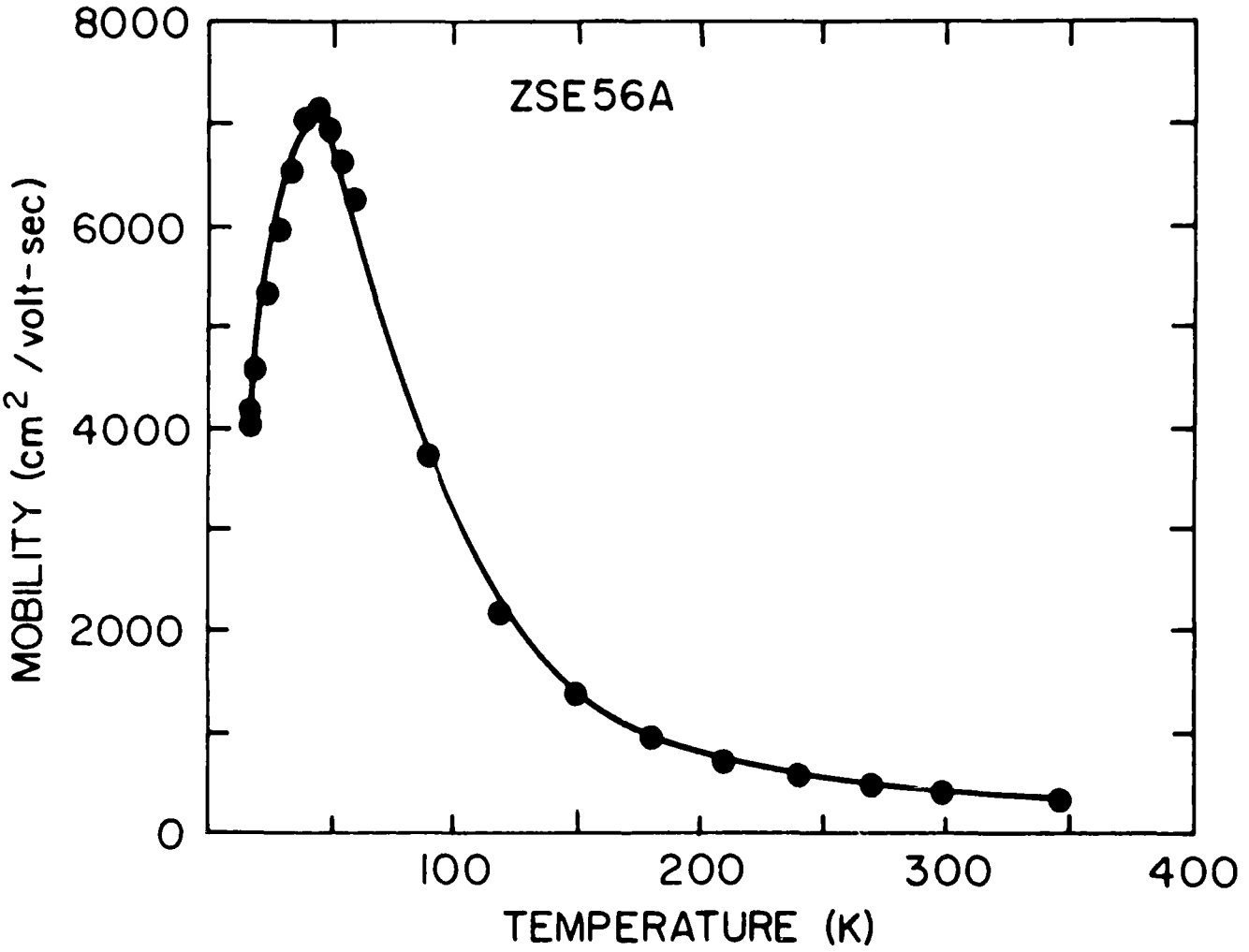

Figure 2-8. Electron Mobility As A Function Of Temperature For ZSE56A. The Peak Mobility Of 7150 cm^{-2}/Volt-Sec Is The Highest Ever Reported For MBE-Grown ZnSe.

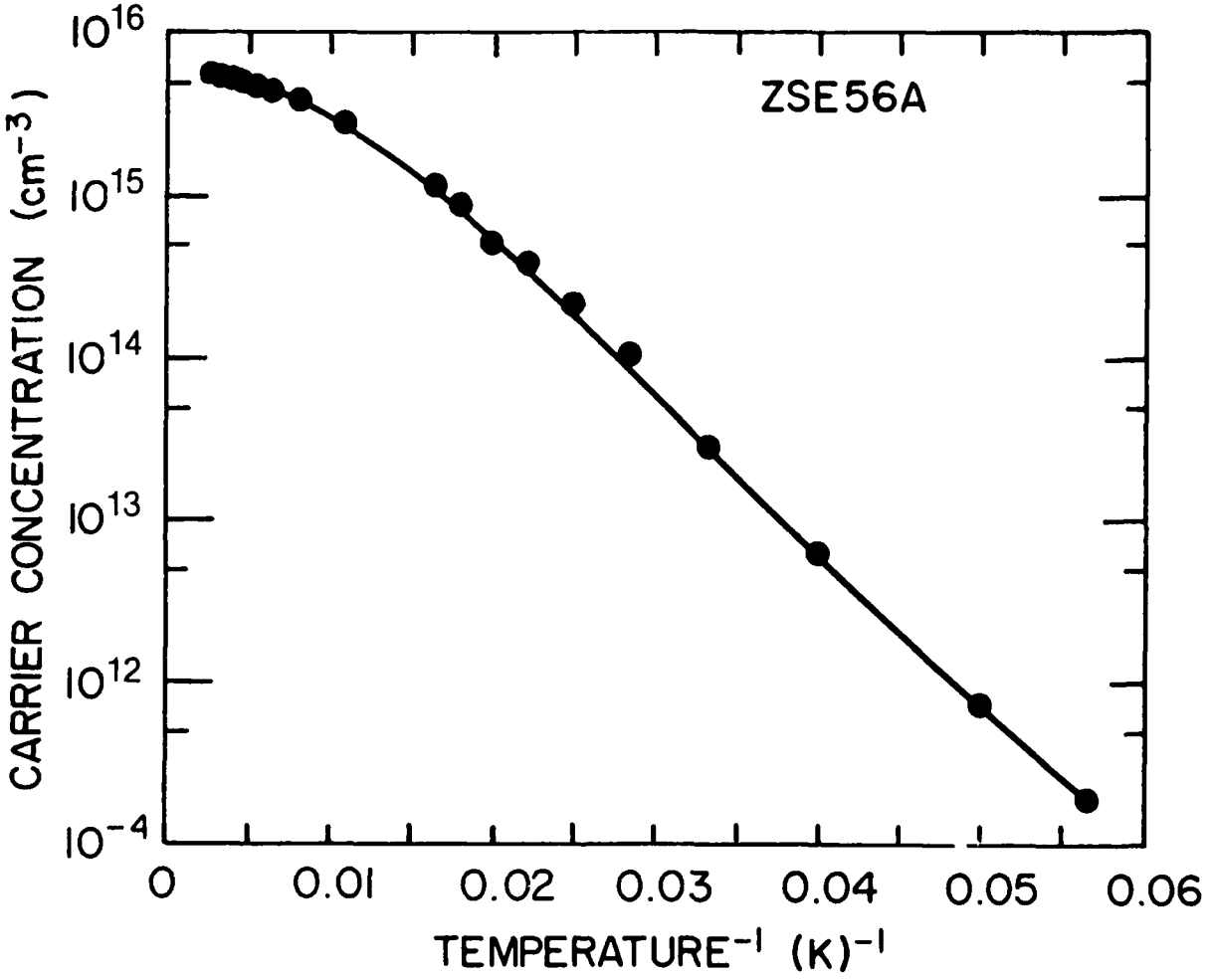

Figure 2-9. Temperature Dependence Of The Carrier Concentration Measured For ZSE56A.

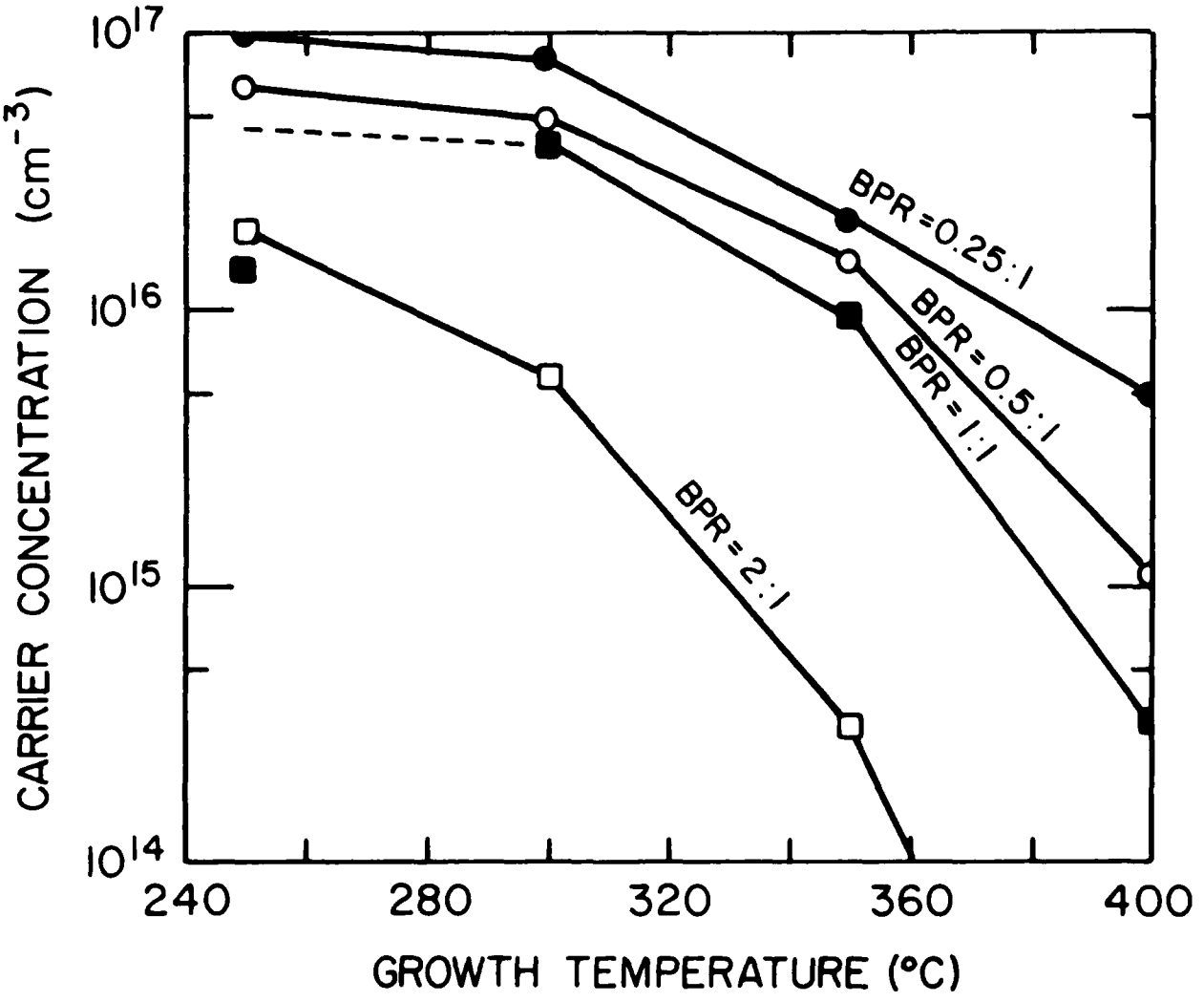

Figure 2-10. Room Temperature Carrier Concentration As A Function Of Growth Temperature For Fixed Zinc:Selenium Beam Pressure Ratios. The Carrier Concentration Monotonically Decreases With Increasing T_g.

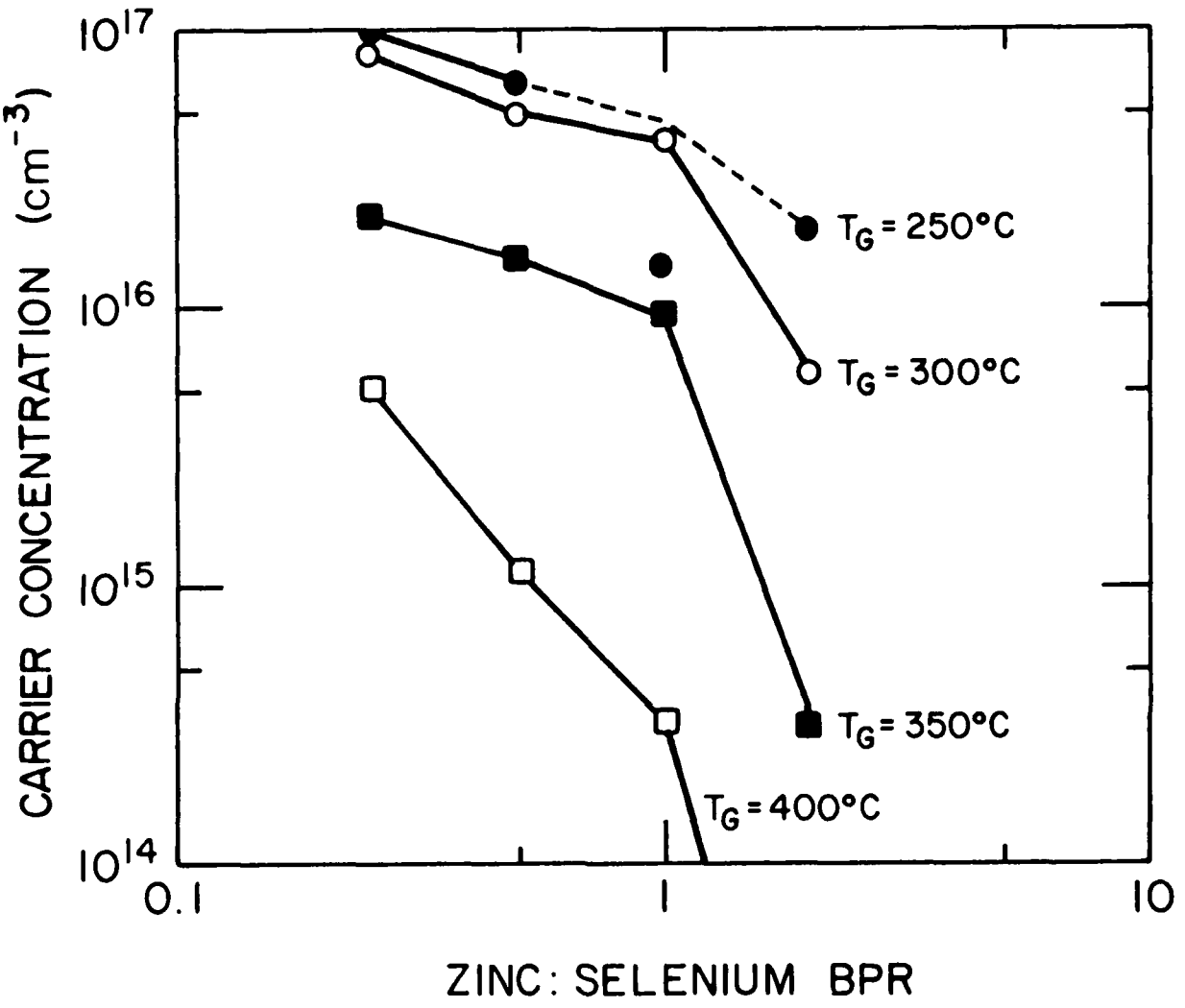

Figure 2-11. Room Temperature Carrier Concentration Plotted As A Function Of Zinc:Selenium BPR For Various Growth Temperatures.

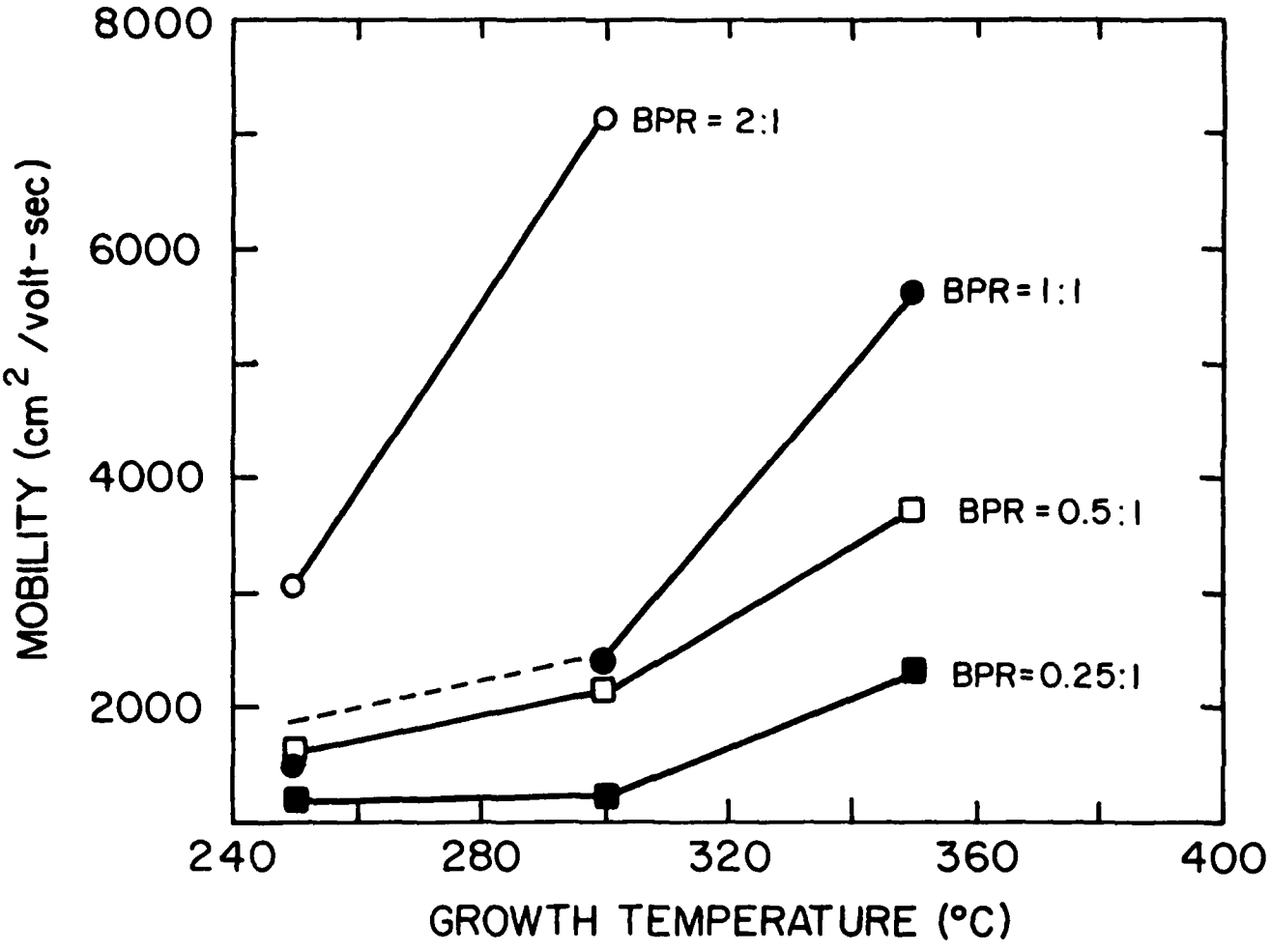

Figure 2-12. Peak Mobility Plotted As A Function Of Zinc:Selenium BPR For Various Growth Temperatures. These Measurements Were Made Using The Van Der Pauw Method With A Magnetic Field Of 2000 Gauss.

When light with energy greater then the bandgap energy is incident upon the sample, free electrons and holes are created. The holes become trapped by the doubly negative sites reducing them to singly negative sites. Singly negative sites have much smaller cross sections than doubly negative sites (roughly by a factor of 4) and thus are much less effective scatterers. The "Photo-Hall" measurements are very preliminary at this time and further investigation of these samples is planned.

2.1.1.4 Capacitance Spectroscopy

Electrical characterization based on Hall measurements gives us information on net shallow donor and acceptor concentrations, carrier concentration, and mobility. This technique, however, does not give useful information on deep levels (electron and hole traps, their energy levels, concentrations and capture cross sections). In the Quarterly Technical Progress Report No. 1, we reported difficulties in obtaining deep level parameters from deep level transient spectroscopy (DLTS) measurements on our ZnSe samples. The DLTS measurement system, however, gave useful deep level information on Si and GaAs. In order to elucidate the system performance, we reported DLTS measurements on a Si-diode in the quarterly report.

During this quarter, we have attempted similar measurements on a series of ZnSe samples. No meaningful information was however obtained. Therefore, we decided to take several alternate approaches for extracting trap parameters. At present, we have initiated capacitance spectroscopy to obtain information on deep traps. In this approach, one measures capacitance as a function of frequency, applied bias and temperature [6, 7, 8]. A typical plot of capacitance vs. frequency and reverse bias voltage for one of our MBE-grown ZnSe samples is shown in Figure 2-13. The low frequency plateau gives the contribution of traps and free carriers to the total capacitance of the depletion layer, whereas the high frequency plateau gives the contribution of free carriers.

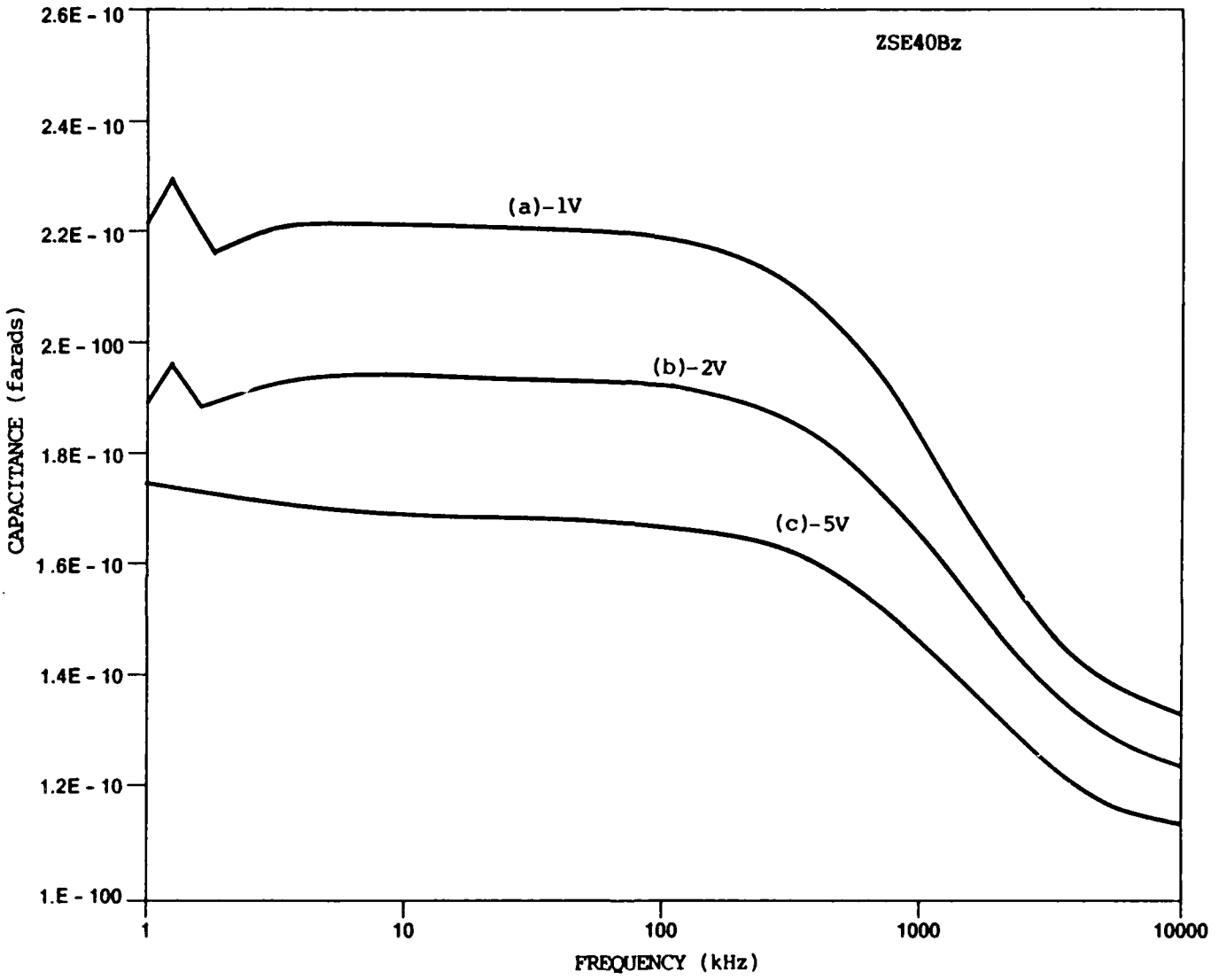

Figure 2-13. Capacitance Versus Frequency For ZSE40BZ For Several Reverse Bias Voltages.

The low frequency capacitance (C_{LF}) can be expressed as follows:

$$C_{LF}^2 = \frac{q\varepsilon N_D}{2\left[V_D - V - \left[\frac{N_T}{N_D}\right]\phi_t\right]}$$

where, q = electronic charge

ε = dielectric constant

N_D, N_T = donor and trap density, respectively

V_D, V = diffusion voltage and applied voltage, respectively

ϕ_t = energy level of the trap

The diffusion voltage was obtained from $1/C^2$ vs. V measurements at 1 MHz (Figure 2-14). With a measured V_D = 1.3 V and N_D = 2.4 x 10^{16}, we obtain $N_T \phi_t \simeq 1.0 \times 10^{16}$, from all the bias dependent C-f measurements shown in Figure 2-13. At present we are carrying out capacitance measurements as a function of temperature to determine trap energy and trap concentrations.

2.1.1.5 Dependence of Surface Morphology on Growth Conditions

The surface morphology of the samples grown for our matrix study has been examined with both dark-field (DFM) and phase-contrast (PCM) optical microscopy. Several surface structures were observed for various samples in this investigation and these structures are defined below:

a) Lines - When a large density of parallel lines is visible over the entire surface of the film. Lines are detected with PCM and are sometimes visible under DFM.

b) Crosshatching - When the surface is covered with lines which intersect at right angles. We have observed crosshatching only with PCM.

c) Stripes - When the surface is striped with regions which appear to have a thickness which is different from the thickness of the neighboring stripe. Stripes have been detected through PCM.

d) Pinholes - When the surface is covered with small random holes or indentations. These are visible with both PCM and DFM.

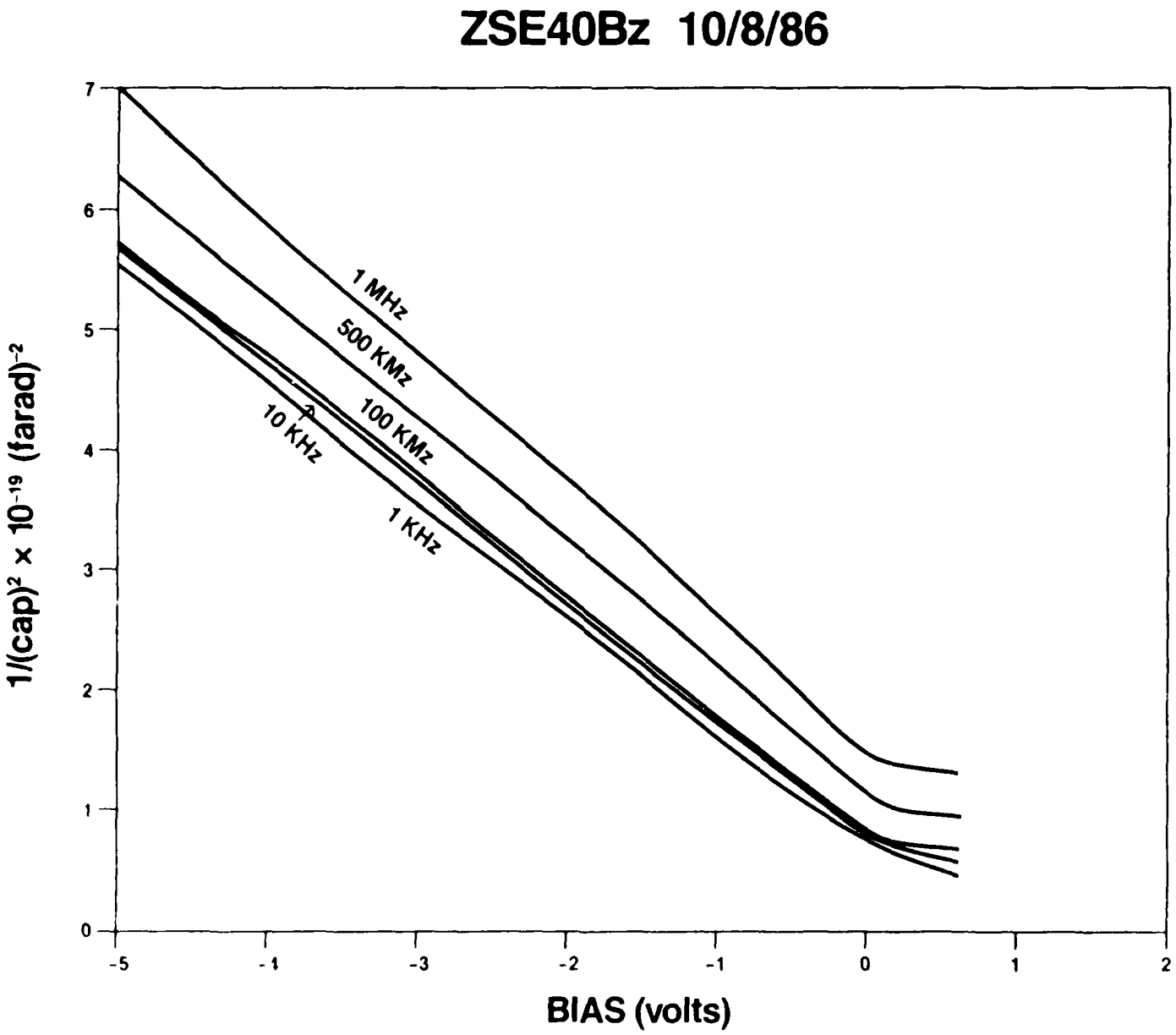

Figure 2-14. $1/C^2$ Voltage For ZSE40BZ At Various Modulation Frequencies.

e) Roughness - In addition to lines, crosshatching, stripes, and pinholes, there exists general surface roughness. This general roughness is difficult to quantify and will be presented as ranging from smooth to very rough.

The results of this investigation are displayed in Table 2-3. The samples which exhibit the best surface morphology lie on a line drawn from (BPR = 1/4:1 , T_g = 400°C) to (BPR = 2:1 , T_g = 250°C). The surface morphology appears to degrade as growth conditions are increasingly altered from those on the indicated diagonal. If surface morphology is included in the determination of the optimum growth conditions then these optimum conditions must lie on or near the diagonal drawn in Table 2-3.

TABLE 2-3. Summary Of Surface Morphology Study. The More Ideal Surfaces Lie On The Diagonal From (1/4:1, 400) To (2:1, 250).

BPR \ T_g	250	300	350	400
1/4:1	Lines Pinholes	Lines rough	Lines and crosshatch Fairly smooth	Faint lines Smooth
1/2:1	Small pinholes	Lines and faint crosshatch Fairly smooth	Very slight crosshatch Smooth	Stripes Slightly rough
1:1	Crosshatch Fairly smooth	Smooth	Small number of lines Fairly smooth	Lines Rough
2:1	Smooth (overgrowth)	Crosshatch Fairly smooth (overgrowth)	Lines Slightly rough (overgrowth)	Extremely rough (overgrowth)

2.1.1.6 Selenium Purification

Improvement in the photoluminescence of ZnSe resulting from selenium source purification has been reported. [9] We have initiated a similar investigation and have completed two selenium purification runs. The starting material used in this study was obtained from SPEX and was specified to contain less than 1 part per million total metallic impurities (1 ppm TMI). In the first purification run, approximately 10 grams of selenium was passed through a three-chamber sublimation cell. Starting

material and "purified" material were submitted to 3M's Analytical Laboratories for analysis. The results of this analysis were inconclusive as the impurity concentration of this material was at or below its detection limit, 1 ppm TMI.

A second purification run utilizing a four-chamber sublimation cell produced approximately 30 grams of selenium in the form of a hemicylinder. The "purified" selenium from this run has been loaded in the selenium source in the MBE system and growth of ZnSe using this selenium will soon begin. The results of this growth run will direct future efforts in this area.

2.1.2 Comparison Of ZnSe Grown On (100) GaAs and (100) Ge

A detailed study was undertaken which was designed to directly compare the ZnSe layer quality with that achieved using both (100) GaAs and (100) Ge as substrate materials. Comparisons have been difficult to make in the past due to differences in in-situ and ex-situ substrate preparation procedures (e.g. thermal-cleaning versus sputter-cleaning) and slight differences in growth parameters. For this set of runs, no chemical etchants were used and both types of substrates were sputtered at room temperature and annealed at 400°C prior to growth. In the case of the (100) GaAs, room temperature sputtering followed by annealing at 400°C was used for the first time as the cleaning technique. The results obtained will now be discussed. Figure 2-15(a) shows the AES spectrum recorded from the "as-loaded" (100) GaAs substrate indicating the presence of O and C contamination. The spectrum is shifted 300 eV to higher energies on account of charging effects. Following 1 hour of sputtering the AES spectrum shown in Figure 2-15(b) was recorded indicating a "clean" GaAs surface. On annealing at 400°C, the RHEED pattern shown in Figure 2-16 was obtained indicating (4 x 1) surface reconstruction. The substrate cleaning results using this technique have been reported previously for Ge. [10]

For the comparative study, two sets of experiments were performed. First, ZnSe layers were grown to a thickness of 2 μ on both (100) GaAs and (100) Ge substrates using a Zn to Se beam pressure ratio of unity at three substrate temperatures in the range 310° to 350°C. Secondly, ZnSe layers were grown to various thicknesses in the range 2 μ to 6.5 μ on both types of substrates using a fixed set of growth conditions; namely, a Zn to Se beam pressure ratio of unity together with a substrate temperature of 330°C.

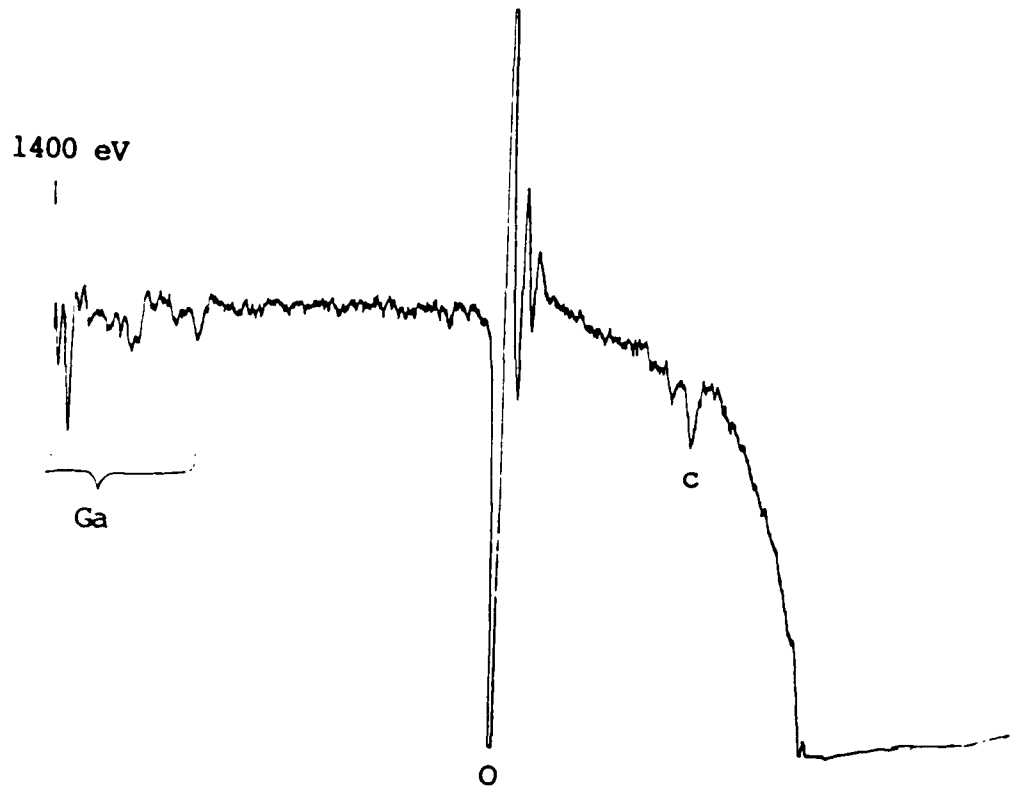

(a) As-Loaded (100) GaAs.

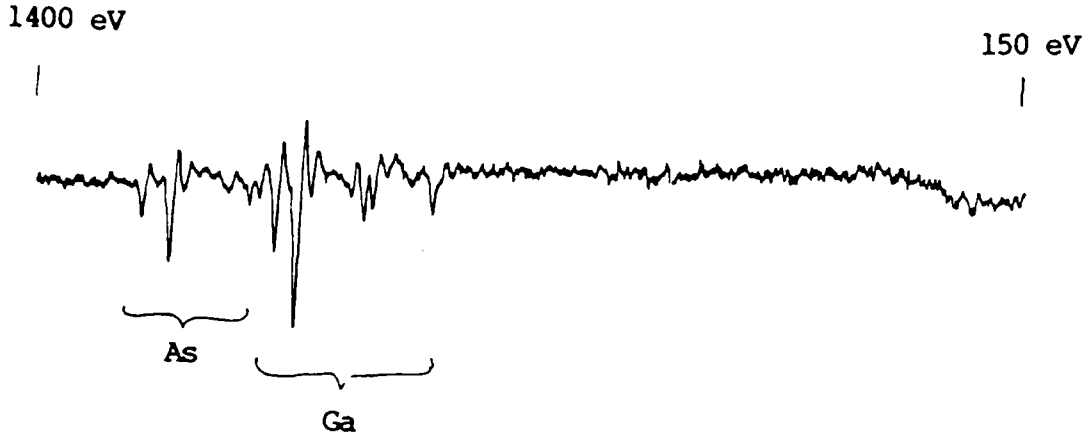

(b) Sputter-Cleaned GaAs.

Figure 2-15. AES Spectra Recorded From (a) An "As-Loaded" (100) GaAs Substrate And (b) GaAs Substrate Following 1 Hour Argon-Ion Sputtering. Spectrum (a) Is Shifted ~ 300 eV To Higher Energies Due To Charging Effects.

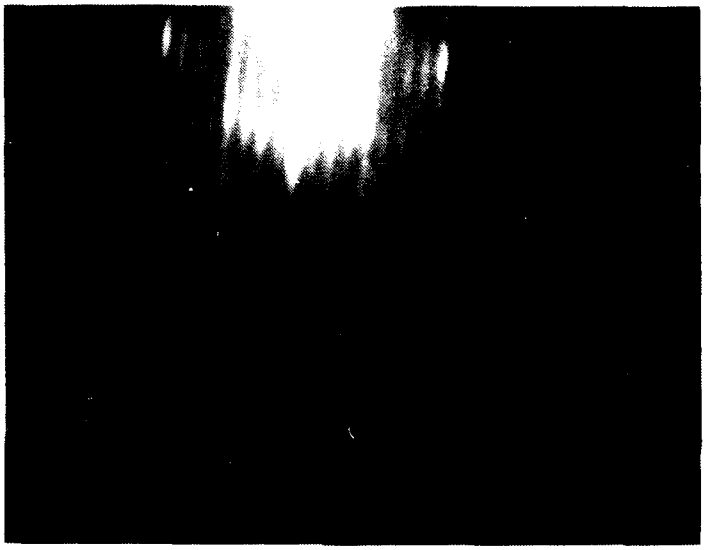

Figure 2-16. A Typical RHEED Pattern Recorded From A RT Sputtered And Annealed (100) GaAs Substrate. The Surface Reconstruction Is (4 x 10).

In addition to the in-situ characterization techniques mentioned above, the ZnSe layers were also characterized using the ex-situ techniques of photoluminescence (PL) and double-crystal x-ray diffractometry. The PL facility has already been described in an earlier report. However, this is the first report of results of double-crystal x-ray diffractometry measurements on our ZnSe layers. The double-crystal x-ray diffractometer made by BEDE, England, was used in the +,- setting of the two crystals; that is, the (100) surfaces of the first and second crystals were aligned parallel to each other. The Cu-$K\alpha_1$ radiation was used as the source of x-rays. The unwanted Cu-$K\alpha_2$ line was cut off using a narrow slit (< 0.5 mm) between the first and second crystals. A GaAs wafer of very low defect concentration supplied by Sumitomo was used as the first crystal. The (400) reflection from the first crystal was used for the measurements. Double-crystal rocking curves (DCRC) were measured of both the epitaxial layers and the substrate.

Of particular concern in this comparative study were the measured PL and DCRC linewidths of the ZnSe layers. Figure 2-17 shows plots of the DBE linewidths measured at 4.2 K for 2 μ thick layers grown on both (100) GaAs and (100) Ge substrates over a range of substrate temperatures. As can be seen from the figure, both curves go through a minimum at a substrate temperature of 330°C, the minimum DBE linewidths achieved at this layer thickness being 0.75 meV and 1.65 meV for growth on (100) GaAs and (100) Ge substrates, respectively. The DCRC linewidths obtained from the 2 μ thick ZnSe layers grown on both substrate types are shown in Figure 2-18. As can be seen from the figure, a substrate temperature of 330° again corresponds to a minimum in the linewidths for both substrate materials, the minimum DCRC linewidths achieved being 176 arc sec. and 437 arc sec. for growth on (100) GaAs and (100) Ge substrates, respectively, at this layer thickness.

Figures 2-19 and 2-20 illustrate plots of DBE and DCRC linewidths as a function of ZnSe layer thickness for layers grown on both (100) GaAs and (100) Ge substrates. As can be seen from the figures, both the DBE and DCRC linewidths for ZnSe/(100) GaAs layers are relatively insensitive to layer thickness over the range 2 μ to 6.5 μ, although both indicate a slight decrease for larger layer thicknesses. On the other hand, the DBE and DCRC linewidths for ZnSe/(100) Ge layers show a relatively strong dependence on layer thickness over the range 2 μ to 6.5 μ.

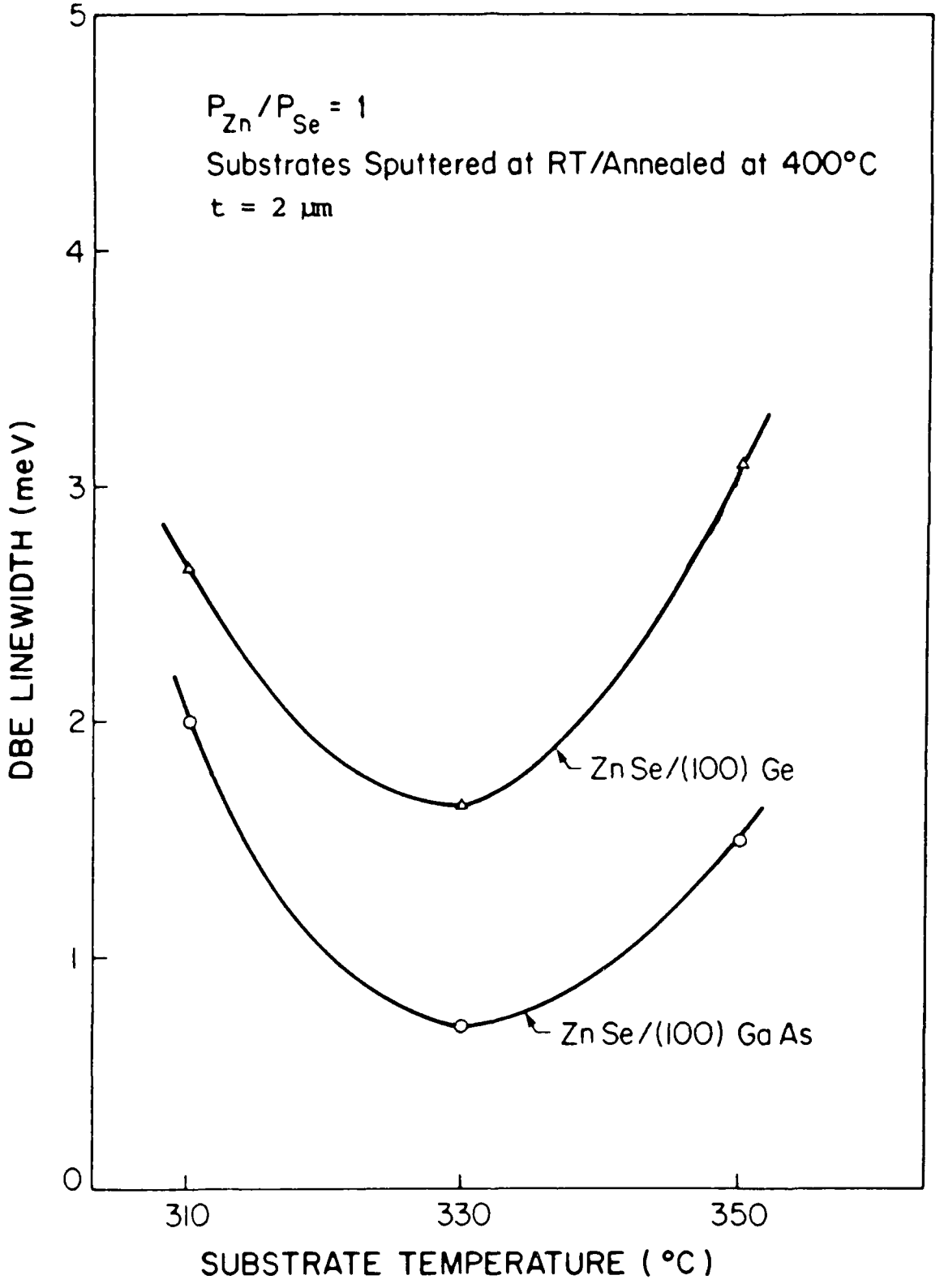

Figure 2-17. Donor-Bound Exciton (DBE) Linewidths Obtained From 2 μ Thick ZnSe Layers Grown On Both (100) GaAs And (100) Ge Substrates As A Function Of Substrate Temperature. A Zn To Se Beam Pressure Ratio Of Unity Was Used Throughout.

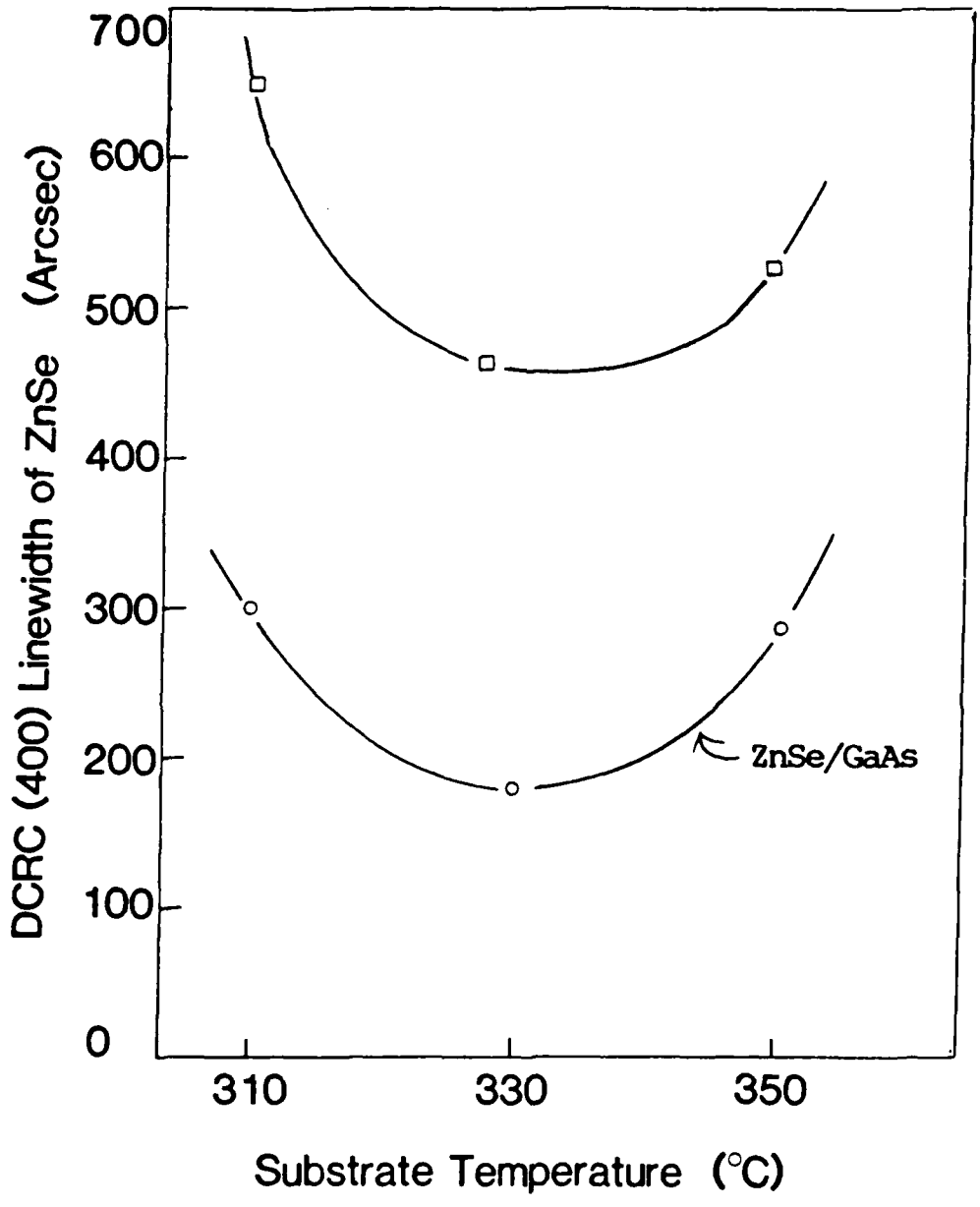

Figure 2-18. Double-Crystal Rocking Curve (DCRC) Linewidths Obtained From 2 μ Thick ZnSe Layers Grown On Both (100) GaAs And (100) Ge Substrates As A Function Of Substrate Temperature.

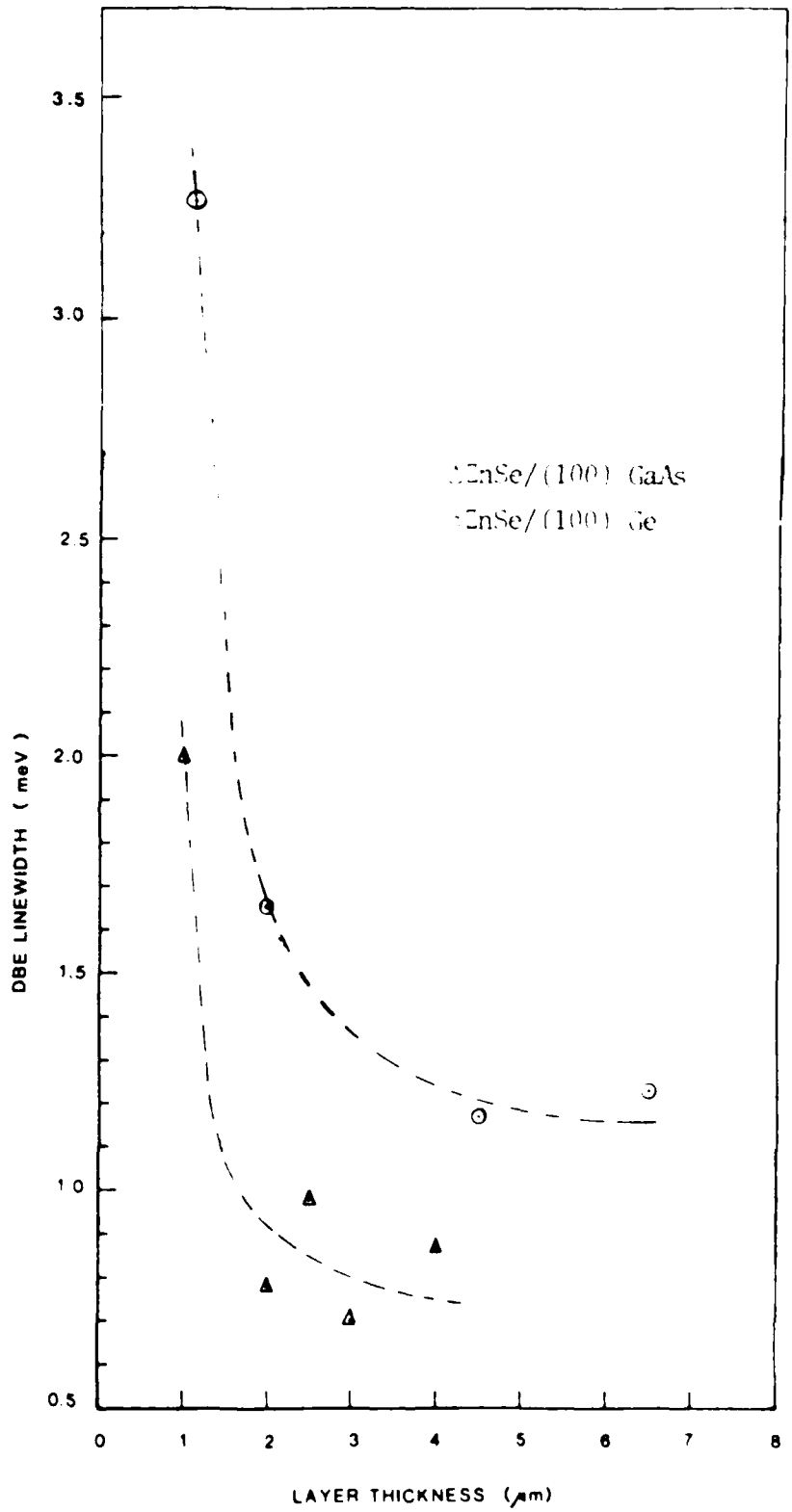

Figure 2-19. DBE Linewidths Obtained From ZnSe Layers Grown On (100) GaAs And (100) Ge Substrates As A Function Of Layer Thickness.

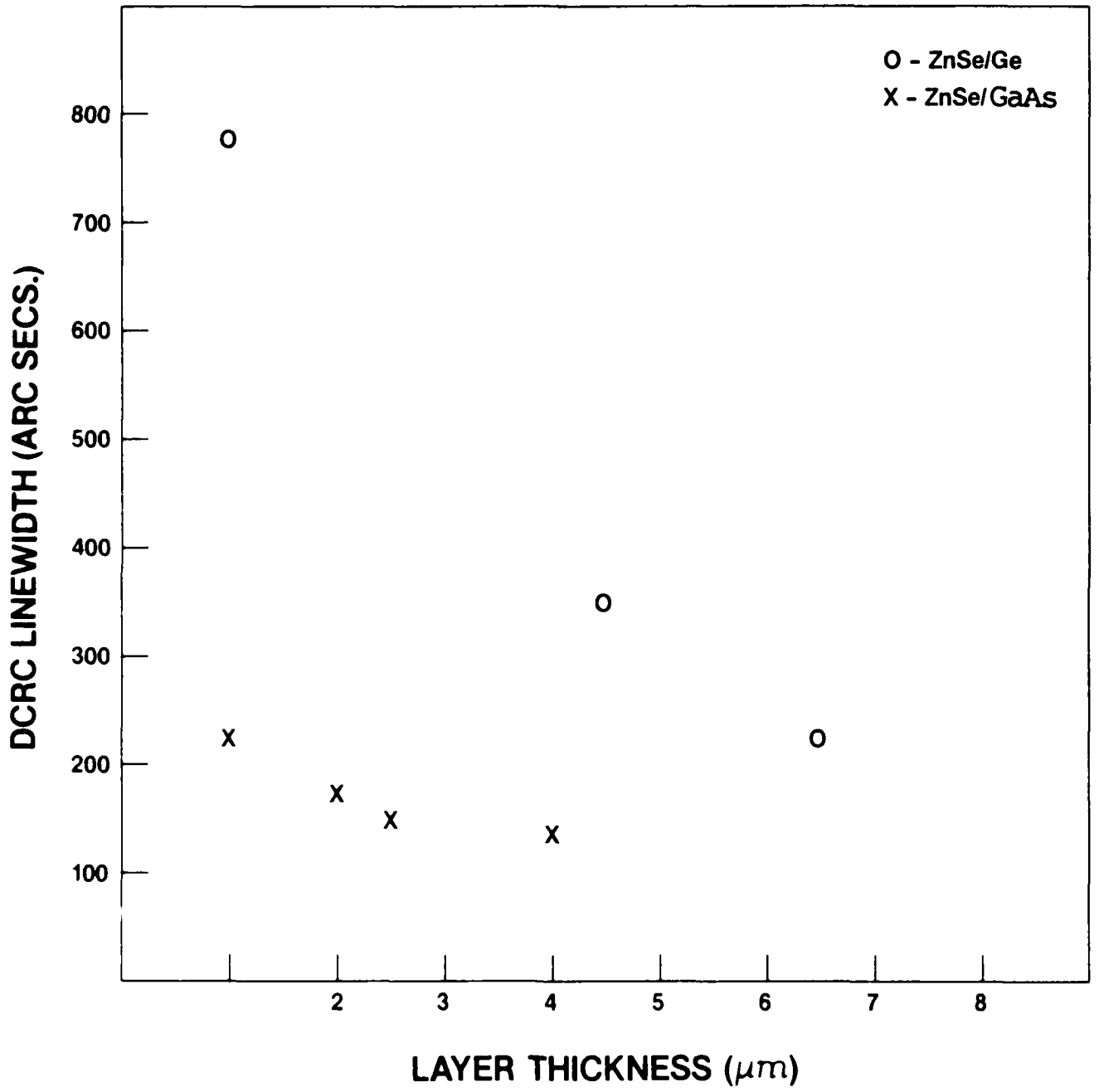

Figure 2-20. DCRC Linewidths Obtained From ZnSe Layers Grown On (100) GaAs And (100) Ge Substrates As A Function Of Layer Thickness.

It can be concluded, therefore, that a lattice relaxation process is taking place over the layer thickness range of 2 μ to 6.5 μ in the material grown on (100) Ge, whereas layers grown on (100) GaAs are already relaxed at a thickness of 2 μ. Furthermore, the above results suggest that ZnSe layers grown on (100) Ge substrates to a thickness of about 6 μ are of comparative quality to those grown on (100) GaAs to a thickness of about 2 μ.

2.1.3 SIMS Analyses

In the fourth quarter, secondary ion mass spectroscopic analyses of ZnSe epitaxial layers were concentrated in four major areas: 1) optimization of analysis conditions in order to increase sensitivity and decrease background in detection of Ga, In and Al, 2) comparison of results for samples grown on Ge substrates with those for samples grown on GaAs, 3) production of ion-implanted standards to quantify analyses for additional species, and 4) preliminary attempts to use the Cs beam for detection of electronegative species.

In order to optimize the analysis parameters for the detection of Ga, In and Al, two separate steps were taken. First, the analyses were done using the maximum possible primary beam current (1 microampere), the largest rastered area (500 microns), the largest analyzed area (250 microns), and the largest secondary ion apertures. This was done in order to maximize secondary ion current, thus maximizing sensitivity and improving counting statistics. Secondly, a systematic study of the effects of voltage offset parameters on mass interferences was begun, in order to minimize the contribution of molecular ions to the background count rate.

Initial attempts to maximize the detected signal by using a large analyzed area resulted in apparent Ga and Al concentrations which were much larger than those reported in the last quarterly report. In some cases, the Ga levels were as much as 1000 times as large, and the Al levels were as much as 100 times as large. Using the imaging capability of the Cameca system, this discrepancy was traced to micron-sized spots of high Ga or Al content. The density of Ga spots was typically a few x 100 cm^{-2}, which was about 10 times that of the Al spots; no In spots were seen. By going to the larger analyzed area to increase signal levels, the probability of including

one of the spots in the field was increased to nearly 1, resulting in higher apparent impurity concentrations. Additionally, it is believed that the spots were responsible for the large scatter seen in earlier analyses done with the smaller analysis area. As a result of this discovery, subsequent analyses done for Al and Ga using the large analyzed area were done by first using the imaging mode to find areas of the sample which were free of spots.

In order to identify the nature of the spots, the SIMS imaging mode was used in conjunction with scanning electron microscopy (SEM) and energy dispersive x-ray analysis (EDAX). First, a Ga or Al spot was located with the SIMS, and then, to better determine the composition of the spot, the mass spectrometer was scanned from mass 8 to 115. The scans showed that Ga and Al spots were often associated with enhanced concentrations of Na, Mg, Si, K, Ca, Ti, Fe, or Cu.

Next, the Ga spots were studied in greater detail. They were marked by focusing the SIMS primary ion beam at two points equidistant from either side of the Ga spot, thus producing craters which marked the spot so that it could be located in the SEM. Subsequent SEM and EDAX analysis of the Ga spots indicated that the the Ga spots were a few microns in size and of two types.

One type consists of a small particle of GaAs which has apparently been deposited on the film surface after growth (see Figure 2-21). Attempts to remove these particles by blowing or washing were unsuccessful. Discussions with other personnel involved in SIMS of semiconductors indicated that the production of adherent particles of substrate material during wafer processing steps, such as cleaving, is commonly observed, and can be minimized by covering the film surface with a protective layer of photoresist until just before analysis. This has not yet been tried on our samples.

Another type of Ga spot consists of a "canyon" in the ZnSe layer (see Figure 2-22), which penetrates all the way to the substrate so that the GaAs surface is observed both in SIMS and EDAX. The edges of the canyon show abnormal overgrowth; it appears that for some reason the ZnSe layer does not begin to grow at a spot a few microns in size. This type of Ga spot appears to be about one-tenth as abundant as the particles, but at this time only a few samples have been analyzed.

Figure 2-21. 7,500X SEM Photo Of GaAs Particle On ZNSe Surface (Bright Spots Are Result Of Composition Analysis By EDAX).

Figure 2-22. 5,000X SEM Photo Of "Canyon" Defect Showing Overgrowth.

No study of the detailed structure of the Al spots has been attempted as yet.

In the course of the SEM work above, a third type of defect, not associated with Ga spots, was discovered. This defect is a circular depression with an appearance reminiscent of craters on the moon (see Figure 2-23). The craters appear to be shallow, and it has not been possible to detect any impurity associated with them. They may be the same defects responsible for the bright spots observed in optical microscopy, and if so, further analysis of these defects could be important in understanding the aging behavior of the ZnSe films, since aging results in an increasing number of bright spots.

For the purpose of determining the optimum voltage offset, a standard technique was used. Curves of detected signal versus voltage offset were taken at the relevant mass numbers on samples of ZnSe/GaAs. This was done using a narrow energy slit. The offset voltage chosen for the analysis was that at which the detected signal became independent of the offset voltage. For the ion species in question, this was typically about 45 volts. Analyses were then performed by opening the energy slit, translating the slit so as to attenuate the Zn mass 64 signal to about 50% of its maximum value, and then using the 45 volt offset.

It was found that the use of the voltage offset had very little effect on the Ga determinations, which is expected, since the most likely mass interference is due to the ZnH molecular ion, which cannot be discriminated by the voltage offset method. The voltage offset also had very little effect on the In determinations; this probably means that there is little molecular interference on the mass 115 signal. In the case of Al determinations, the voltage offset produced a marked effect, reducing the estimated Al content by over an order of magnitude. This is to be expected , since the primary interference here should be due to hydrocarbons, which can be removed by the offset technique.

Using the maximum primary ion current, largest analysis area, 45 volts offset, and choosing spots that were free of Ga and Al spots, samples number ZSE 12,13,14, and 15 were re-analyzed. The results of the analyses are summarized in Table 2-4. It can be seen that the Ga and In values are in good agreement with the values given in Quarterly Technical Progress Report No. 1, Section 2.1.5., while the Al values are considerably lower.

TABLE 2-4. Revised SIMS Upper Limits On Ga, In, and Al Concentrations.

Sample	Measured N_D (cm^{-3})	[Ga] Max. (cm^{-3})	[In] Max. (cm^{-3})	[Al] Max. (cm^{-3})
ZnSe/GaAs:				
#12	2.2×10^{17}	2×10^{15}	2×10^{14}	1×10^{14}
#13	9.0×10^{16}	3×10^{15}	1×10^{14}	1×10^{14}
#14	7.1×10^{16}	2×10^{15}	1×10^{14}	4×10^{14}
#15	2.5×10^{16}	4×10^{15}	5×10^{14}	1×10^{15}
ZnSe/Ge:				
# 7	?	1×10^{15}	9×10^{14}	4×10^{16}
#14	?	2×10^{15}	5×10^{14}	2×10^{15}

Figure 2-23. 10,000X SEM Photo of "Crater" Defect.

In order to check for any differences in contamination between ZnSe layers grown on GaAs in the St. Paul MBE system and ZnSe layers grown on Ge in the Toronto system, ZnSe/Ge samples number 7 and 14 were analyzed under the same conditions. The results of these analyses are also presented in Table 2-4. The Ga and In values for the Ge substrate samples are in good agreement with the values for the GaAs substrate samples, but the Al values are consistently higher. This could be due to more Al in the starting material used for the films grown in Toronto, but might also be due to stronger hydrocarbon interference or irreproducible discrimination in the voltage offset technique. It is noteworthy that the mass 27 signal is more strongly enhanced at the surface of the Ge substrate films than at the surface of the GaAs films--this would be consistent with surface hydrocarbon contamination.

Two important conclusions can be drawn from the above results: First of all, given the fact that the measured donor concentrations in the ZnSe/GaAs samples are large compared to the Ga, In and Al concentration upper limits these elements alone cannot account for the n-type behavior of the material (at least not in the relatively low resistivity material studied to date). Secondly, because no difference can be detected in the Ga and In contents of the samples grown on GaAs with In as a bonding agent and the Ga and In contents of the samples grown on Ge without In solder, it may be concluded that the amount of Ga introduced into the films as a result of diffusion from the substrate, and the amount of In introduced from the solder, are negligible.

In addition to the Ga, In and Al efforts discussed above, preparations were made for SIMS studies of other contaminants and dopants. Ion-implanted ZnSe/GaAs standards for quantification of F, Cl, and As contamination, as well as N and Na doping, were obtained.

Some preliminary attempts at using the Cs primary beam and negative secondary ion detection in analyses for F, Cl and As were made. However, in attempting to follow implantation profiles of these species, very large background signals were observed. Initial attempts to enhance the signal-to-background ratio using voltage offset were unsuccessful, but these were cut short due to failure of the electron multiplier.

In the next quarter, the electron multiplier will be replaced, after which studies of F, Cl, and As detection will continue. Ion-implanted standards for other likely contaminants such as C, O, Si, Ge, and Cu will be obtained. Studies of intentional dopants such as N and Na will begin. Perhaps most importantly, a general program to better characterize and optimize the voltage offset technique, and thus to achieve the best possible detectability limits in the presence of molecular interferences, will be pursued.

2.1.4 Theory of N-ZnSe Materials Characterization By Free Carrier Absorption

ZnSe with its direct bandgap of 2.7 eV at room temperature has the potential to become an important material for the fabrication of efficient blue light-emitting devices. The realization of this potential, however, hinges on an ability to control the electronic properties of the material. Free carrier absorption (FCA) measurements provide information directly on perturbations to the crystal lattice (by both phonons and impurities) and consequently FCA offers an excellent means of probing material quality. FCA has an inherent advantage over Hall-Effect measurements in being contactless, and therefore completely non-destructive. An exact and inclusive theory of FCA in n-ZnSe can accelerate progress towards attaining ZnSe material of a quality suitable for the next generation of light-emitting devices.

This work [11] is the first report of a treatment of FCA in n-ZnSe to include all major scattering mechanisms, and to solve for the FCA coefficients exactly under generalized Fermi-Dirac statistics. The necessity to resort to an exact quantum theoretical model for FCA is dictated by the inapplicability of classical FCA theory. This originates from the fact that typical photon energies are comparable to electron energies at 300 K; therefore, the fundamental assumption of classical theory that electrons can quasi-continuously gain energy from the electromagnetic field, is violated.

The contribution of all major scattering mechanisms to the total FCA is given in Figure 2-24 for a probe wavelength of 10 μ. As was the case in both electron [12] and hole [13] transport in ZnSe, polar optical phonon scattering is the dominant scattering mechanism.

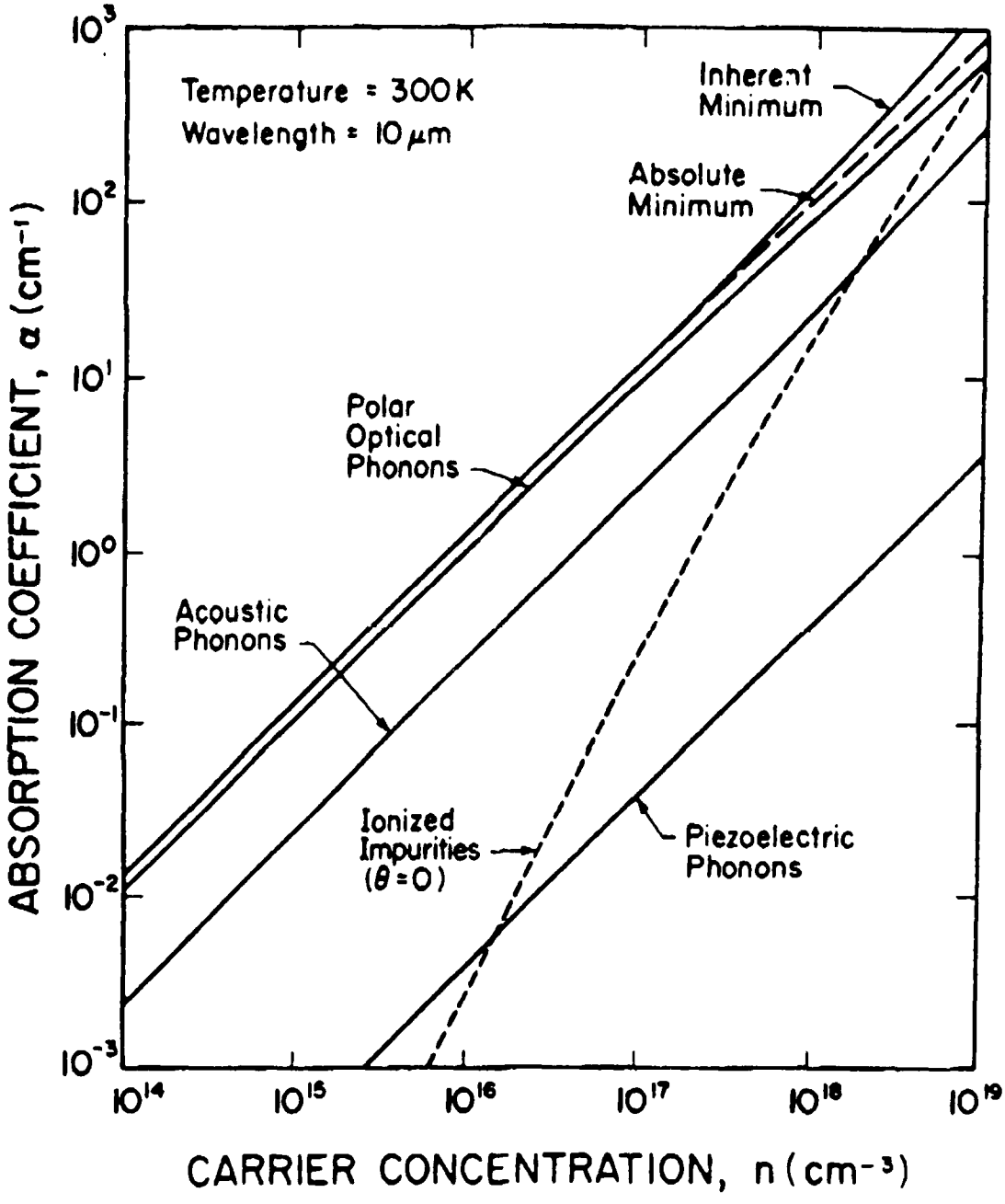

Figure 2-24. Calculated Component Contributions To FCA Vs. Carrier Concentration At 10 μ At 300 K. Ionized Impurity Curve Is Calculated At $\theta = 0$.

An inherent minimum absorption coefficient, α_{inh} is given in Figure 2-24 corresponding to totally uncompensated material. The equation for this limit may be written as log α_{inh} (cm^{-1}) = log n (cm^{-3}) - 15.9 for $10^{14} \leq n(cm^{-3}) \leq 10^{17}$. Furthermore, the influence of the compensation ratio and ionized impurity density were calculated. These relations were derived for λ = 3.3 μ 5 μ and 10 μ respectively, and can be compared with experimental data from the literature, as can be seen in Figure 2-25. The derivative logarithmic absorption coefficient, p, given in Figure 2-26 was shown to be an important parameter, which when used in conjunction with α_{expt} yielded carrier concentration values directly through the relation, n (cm^{-3}) = 6.7 x 10^{15} (3.5 - p) α_{expt} (cm^{-1}). Calculated n values are in excellent agreement with experimentally determined values (from Hall-Effect measurements) reported in the literature. The calculated curves of p(n) at different values yield θ values directly. Thus a straightforward method of evaluating n and θ from experimentally obtained p and α_{expt} data values is possible. This approach may be easily adapted to provide the basis for a microscale mapping of n and θ values in n-ZnSe by employing a rastered laser based absorption experiment.

2.2 Project II, Task 1: Device Research, Photopumping, e-Beam Pumping And Cavity Formation

2.2.1 e-Beam Pumping Measurements

For the greater part of this quarter, our electron beam system was undergoing repairs. Most of the delay was due to the vendor's redesigning and testing a new firing unit in attempt to alleviate some of the problems which have caused us to burn up four filaments in the past eight months. The system has now been reinstalled, tested and recalibrated, and we have made several series of measurements on new samples, most notably #ZSE48A which is 4.3 μ thick. This is the first time we have looked at a thick sample, and the results are quite encouraging. Since we can now work at higher accelerating voltages, we have been able to observe lasing all the way up to room temperature! Figure 2-27 shows the room temperature spectra obtained under increasing beam current density; the onset of lasing at J_{th} = 10 A/cm^2 can be seen clearly.

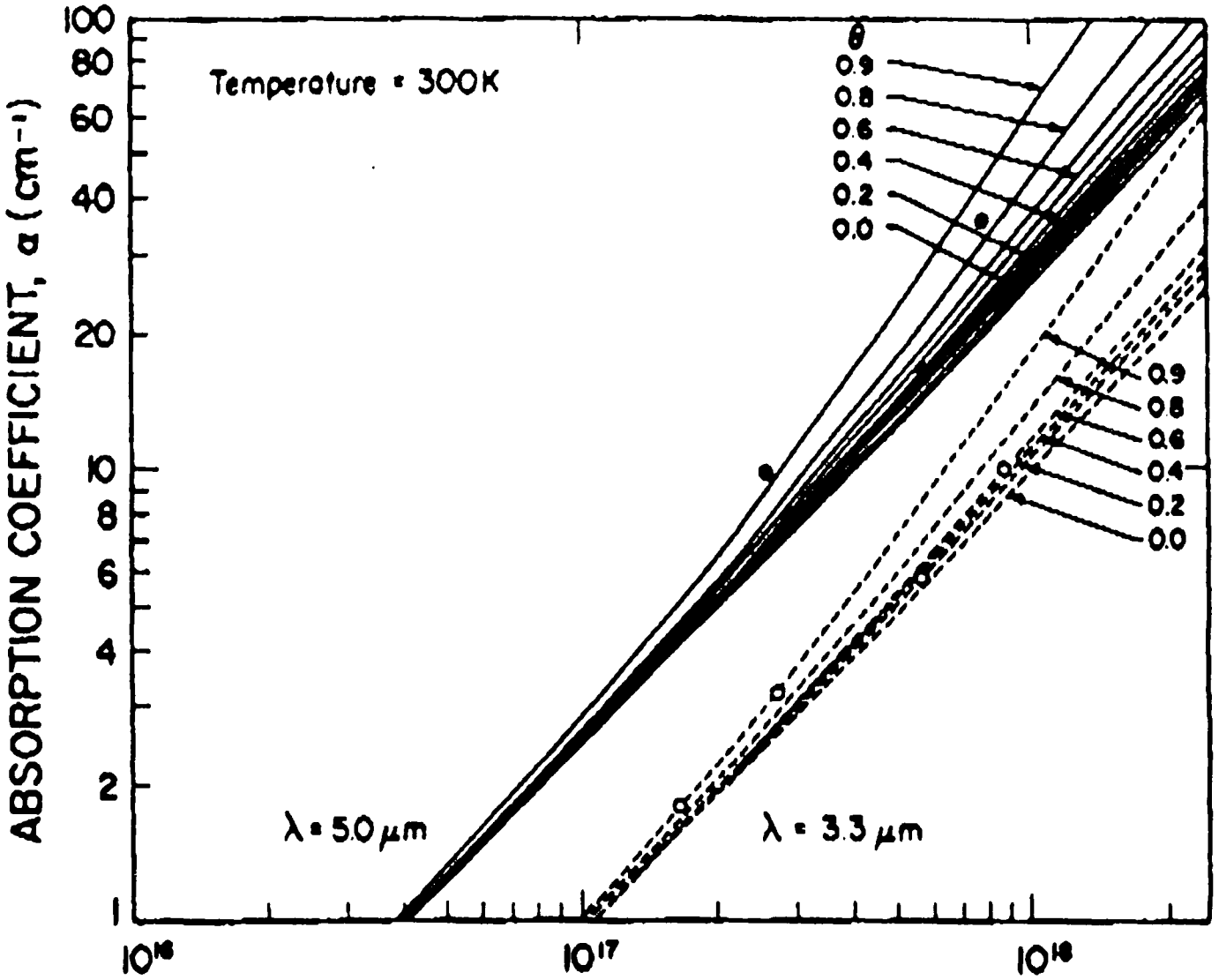

Figure 2-25. Calculated Total FCA VS. Carrier Concentration Given As a Function Of θ For λ = 3.3 and 5.0 Microns.

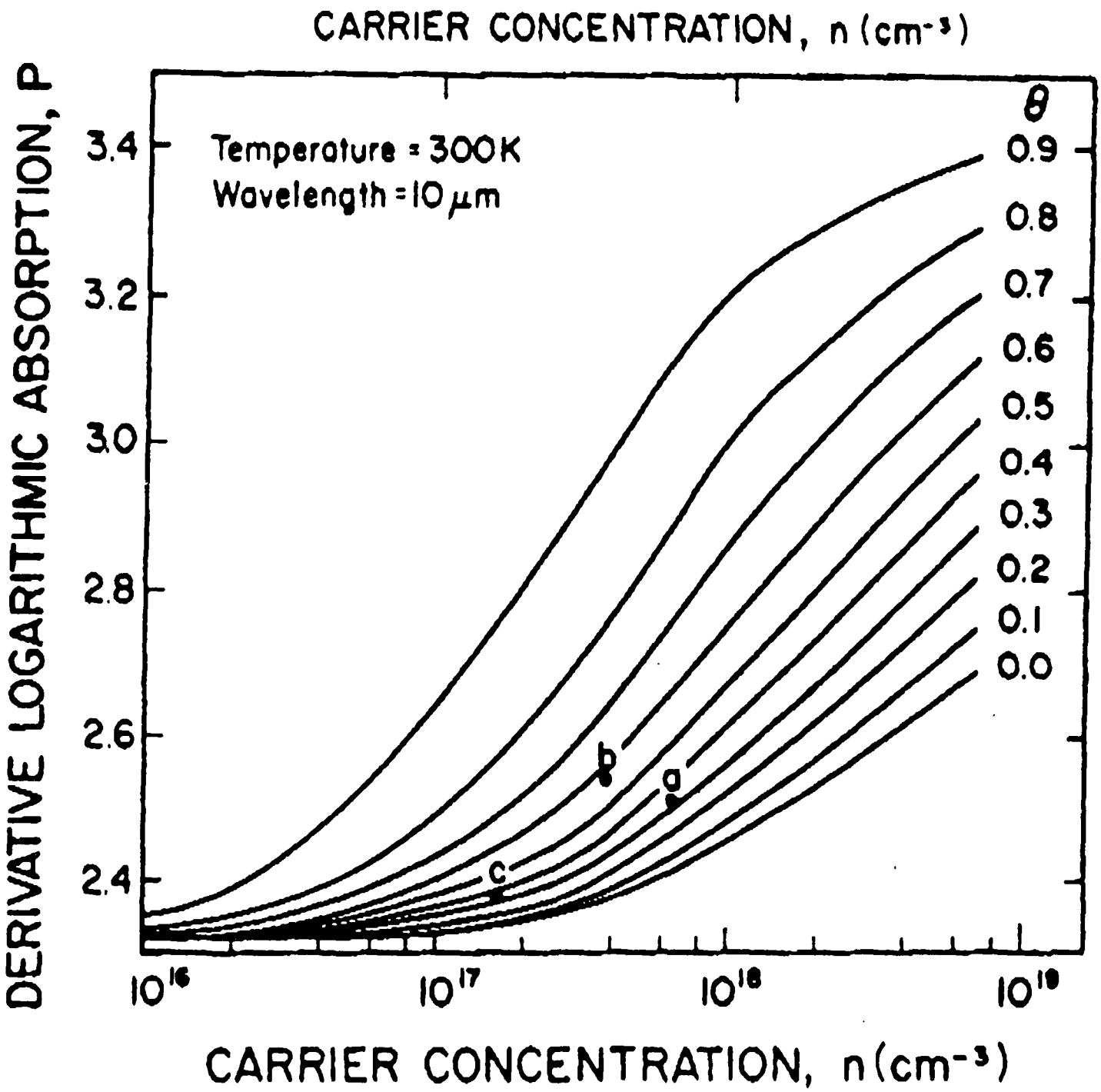

Figure 2-26. Calculated Curves Of The Derivative Logarithmic Absorption Coefficient p Vs. Carrier Concentration Given As A Function Of θ At 10 Microns.

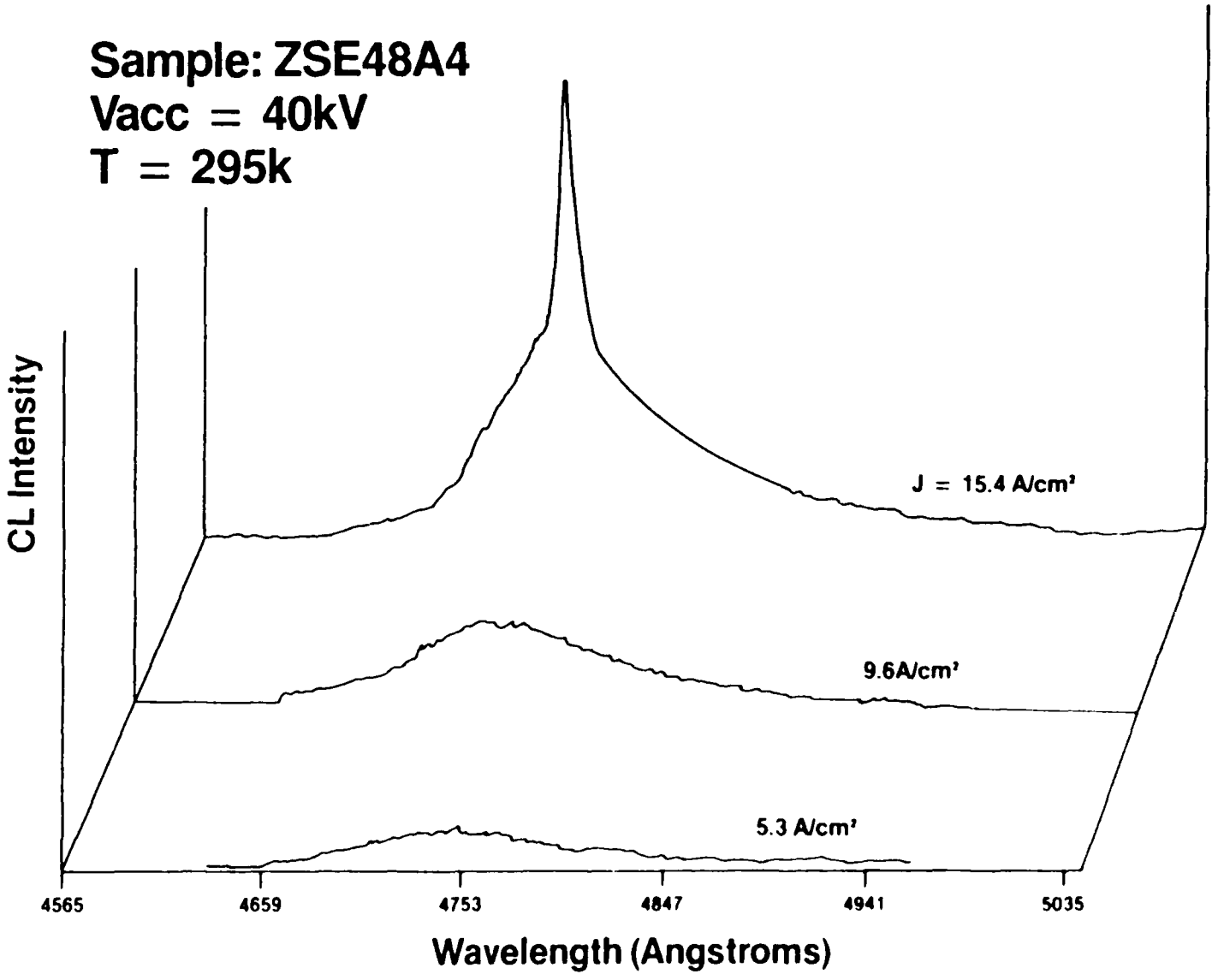

Figure 2-27. Spectral Output Of Sample #ZSE48A Under Electron Beam Excitation At The Current Densities Indicated. This Is The First Reported Observation of Lasing In An Electron-Beam-Pumped MBE ZnSe Film.

While the 16 K, 20 kV threshold is higher than we have seen in some samples (approximately 8 A/cm^2 compared with values as low as 3.9 A/cm^2 observed previously with a different sample), the threshold decreases by better than a factor of four on increasing the accelerating voltage to 40 kV [see Figure 2-28(b)]. This behavior should be contrasted with that which we reported earlier (see our Quarterly Technical Progress Report No. 1) for a 2.0 μ thick sample where we found the threshold rising for accelerating voltages greater than 20 kV due to penetration of the electron beam into the GaAs substrate. At 40 kV, the threshold increases by a factor of 3-4 over the temperature range from 16 K to 300 K [see Figure 2-28(b)]. We feel that better control of the cavity formation and sample mounting procedures will bring the 20 K, 20 kV threshold back down to approximately 4 A/cm^2. Working at 40 kV, we will then have thresholds in the vicinity of 1 A/cm^2; this will certainly help to prolong the life of the e-gun's cathode and reduce our down time.

During the next quarter we will be devoting some time to identifying the mechanism for lasing in these materials in different temperature and current density regimes. This will entail making very careful measurements of the time evolution of the light output using a boxcar integrator for obtaining higher time resolution than is possible with the optical multichannel analyzer. We will also try to correlate the threshold with other optical and electrical properties which we are measuring for these samples. Finally, we will be looking at the dependence of the lasing threshold on the cavity length and on the facet reflectivity.

2.3 Project II, Task 2 - Contact Studies

2.3.1 Contacts - Ohmic and Schottky

In all the capacitance-voltage measurements so far, a Schottky barrier was fabricated on ZnSe grown on n^+GaAs substrate. Because of the difficulty in fabricating ideal Schottky barriers on air-exposed samples, we decided to fabricate indium ohmic contacts on ZnSe grown on p^+ and n^+GaAs substrates. The purpose of ohmic contacts was twofold: 1) to determine interface band bending which determines carrier transport at the interface, and 2) to determine deep level parameters in In/ZnSe/p^+GaAs structures. In the last quarterly report, we reported a method of fabrication of ohmic contacts out of evaporated indium.

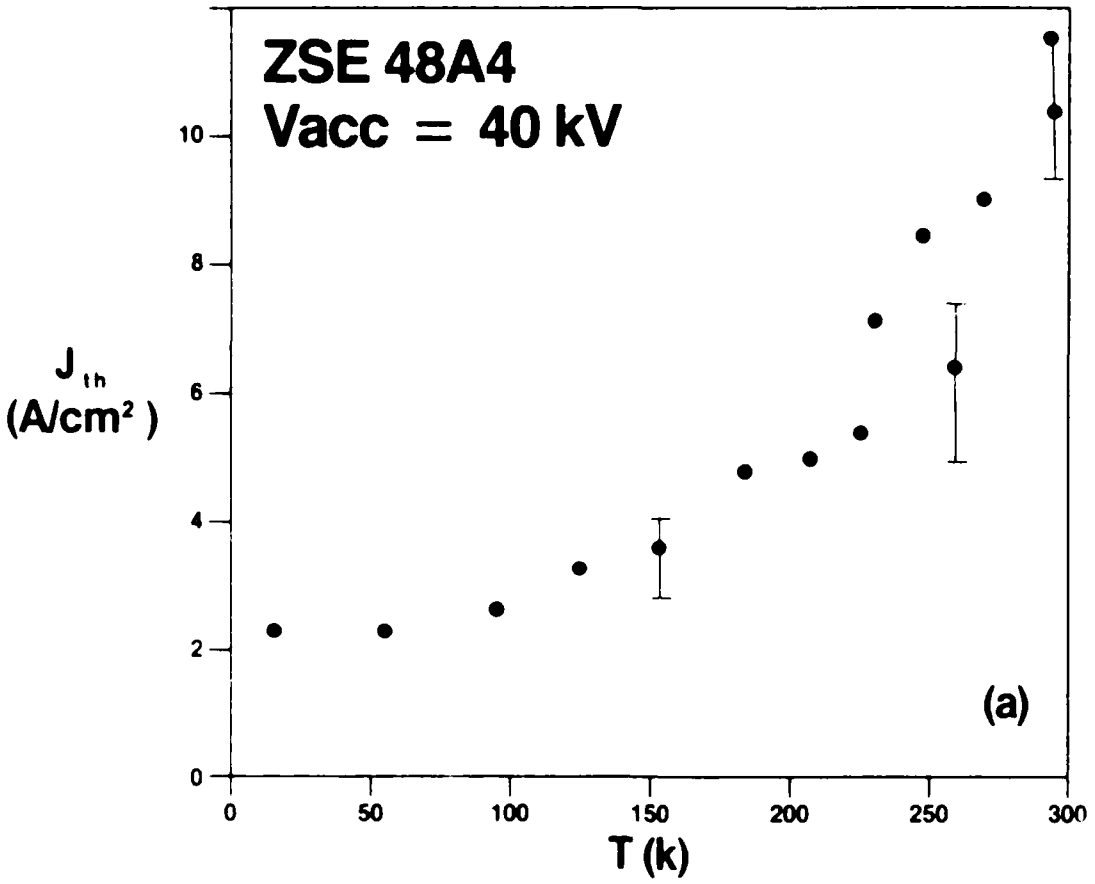

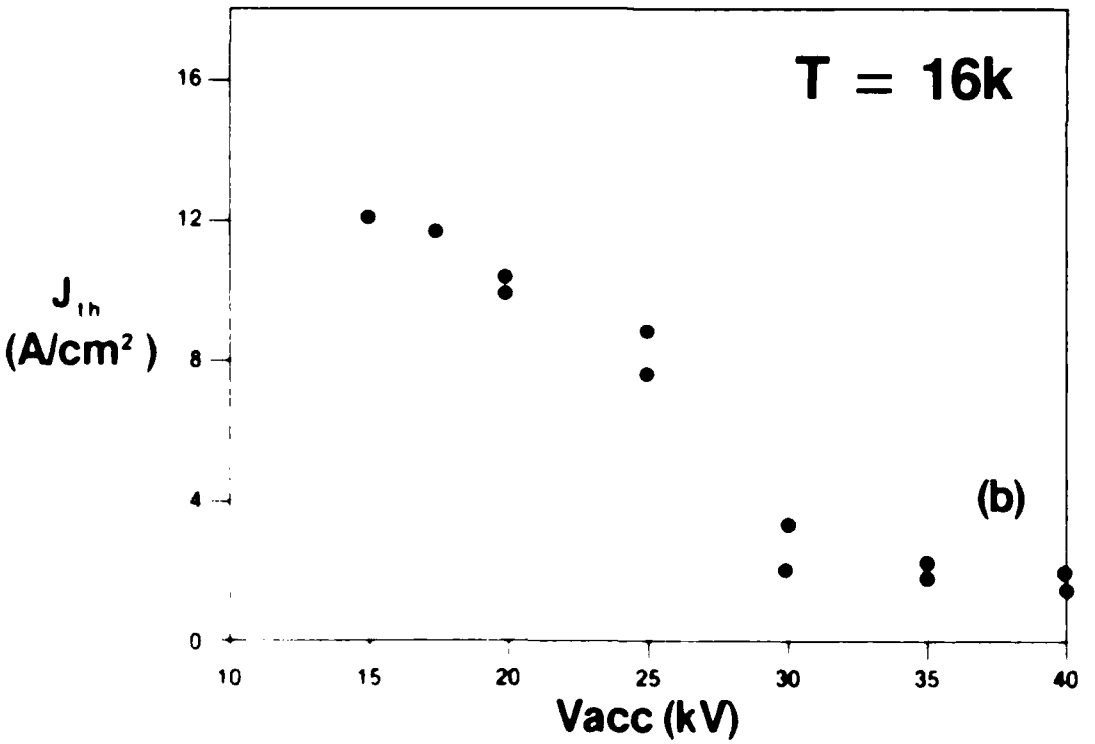

Figure 2 28. Dependence Of The Threshold Current Density On Sample Temperature For Sample #ZSE48A4 Measured At 40 KV. Dependence Of The Threshold Current Density On The Electron Accelerating Voltage Measured At 16 K.

While repeating the process, we ran into reproducibility problems. In all cases, In (~ 500 Å) was deposited on ZnSe grown on semi-insulating GaAs in a diffusion-pump-based system at a base vacuum of 2.3×10^{-7} Torr. Invariably. In gave a rectifying behavior (Figure 2-29) even after prolonged annealing in flowing Ar/H_2 (95/5) gas. From $1/C^2$ vs. V plots (Figure 2-30) for the In/ZnSe/n^+-GaAs/In structure, a barrier height of 1.4 V was obtained. With prolonged annealing, this remained unchanged. Surprisingly, a similar barrier height was also observed on aluminum Schottky barriers from our earlier measurements. This value of the barrier height (ϕ_B) is ~ 0.6 eV higher than that reported in the literature [14]. This large ϕ_B is probably due to an interfacial oxide. We are in the process of fabricating ex-situ sputtered contacts on ZnSe in order to eliminate the interfacial oxide.

Annealing of In under a high flow rate of Ar/H_2, resulted in a yellow surface discoloration of the In. Subsequent Auger depth profiling (Figure 2-31) measurements indicated the presence of oxide on the surface of the In. However, when the evaporated In was annealed at 220°C in the presence of additional In metal, the contacts became ohmic. Due to the absence of evidence to the contrary, we attribute the rectifying behavior to formation of islands by the evaporated In, and to oxidation of the In surface.

Recently we deposited an aluminum protective layer over indium without breaking the vacuum. As deposited, this gives a very high resistive contact. Current-voltage characteristics as a function of annealing time is shown in Figure 2-32. With prolonged annealing, the contact characteristics however degraded. We repeated this process on two different samples and obtained better Ohmic contacts. The extent of indium diffusion into ZnSe has not been determined yet. In the next quarter we will further investigate on ex-situ Ohmic and Schottky contacts on ZnSe.

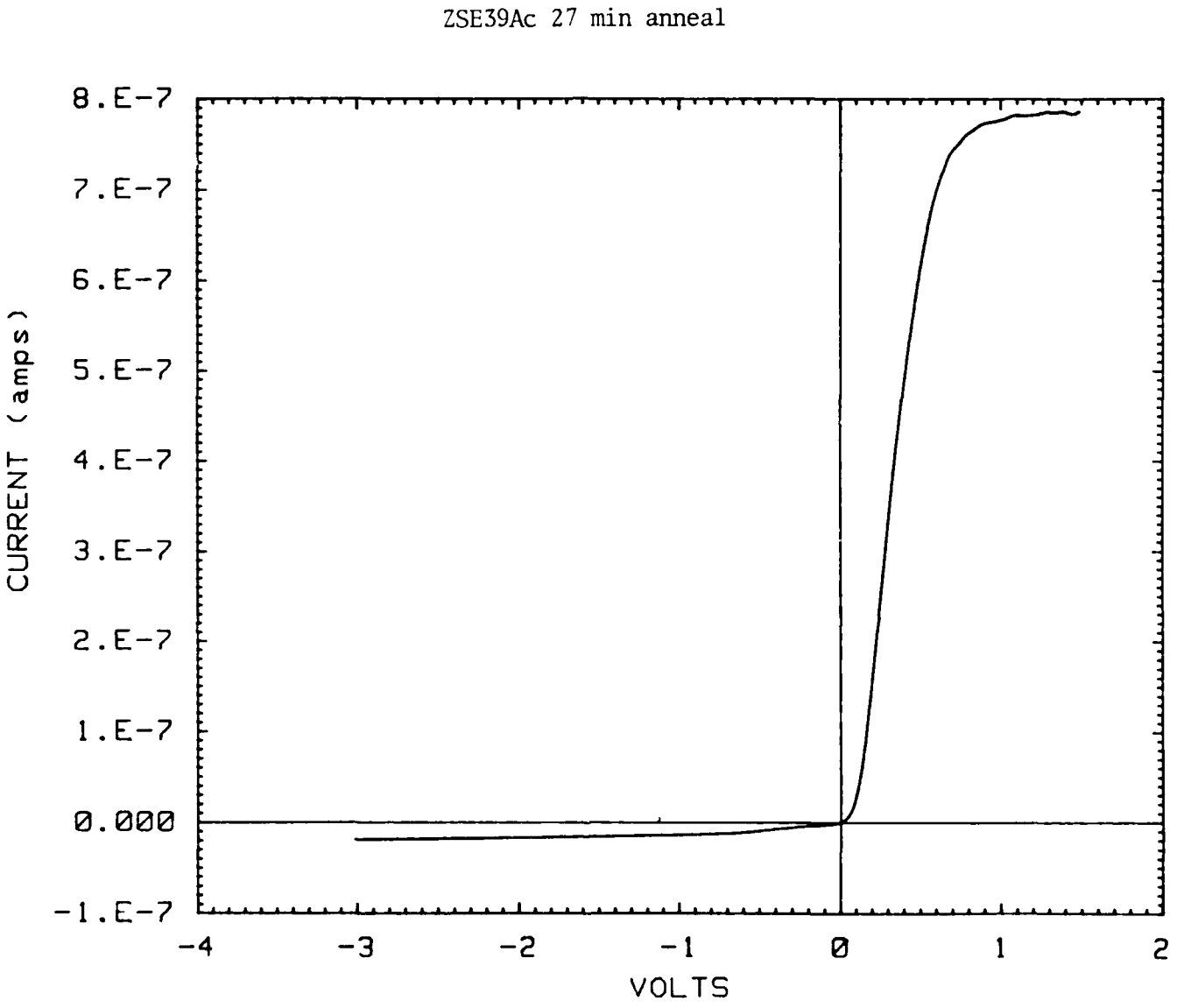

Figure 2-29. Current-Voltage Characteristics Of Annealed Indium Contacts on ZnSe/S.I. GaAs.

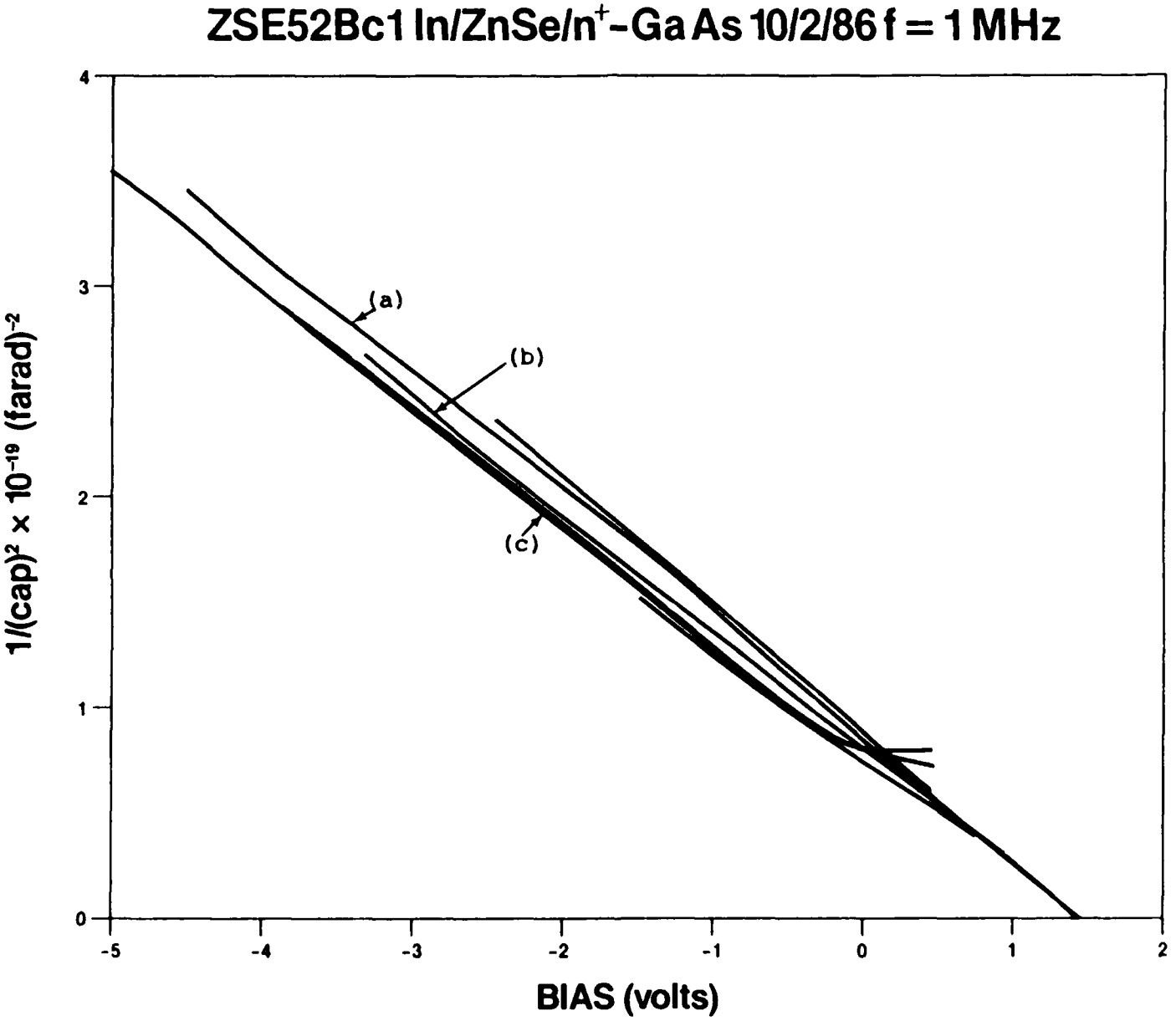

Figure 2-30. $1/C^2$ Versus V For In/ZnSe/n+GaAs As A Function of Annealing Time (T=210°C): (a) Unannealed, (b) 1/2 Hour Annealed, (c) 1 Hour Annealed.

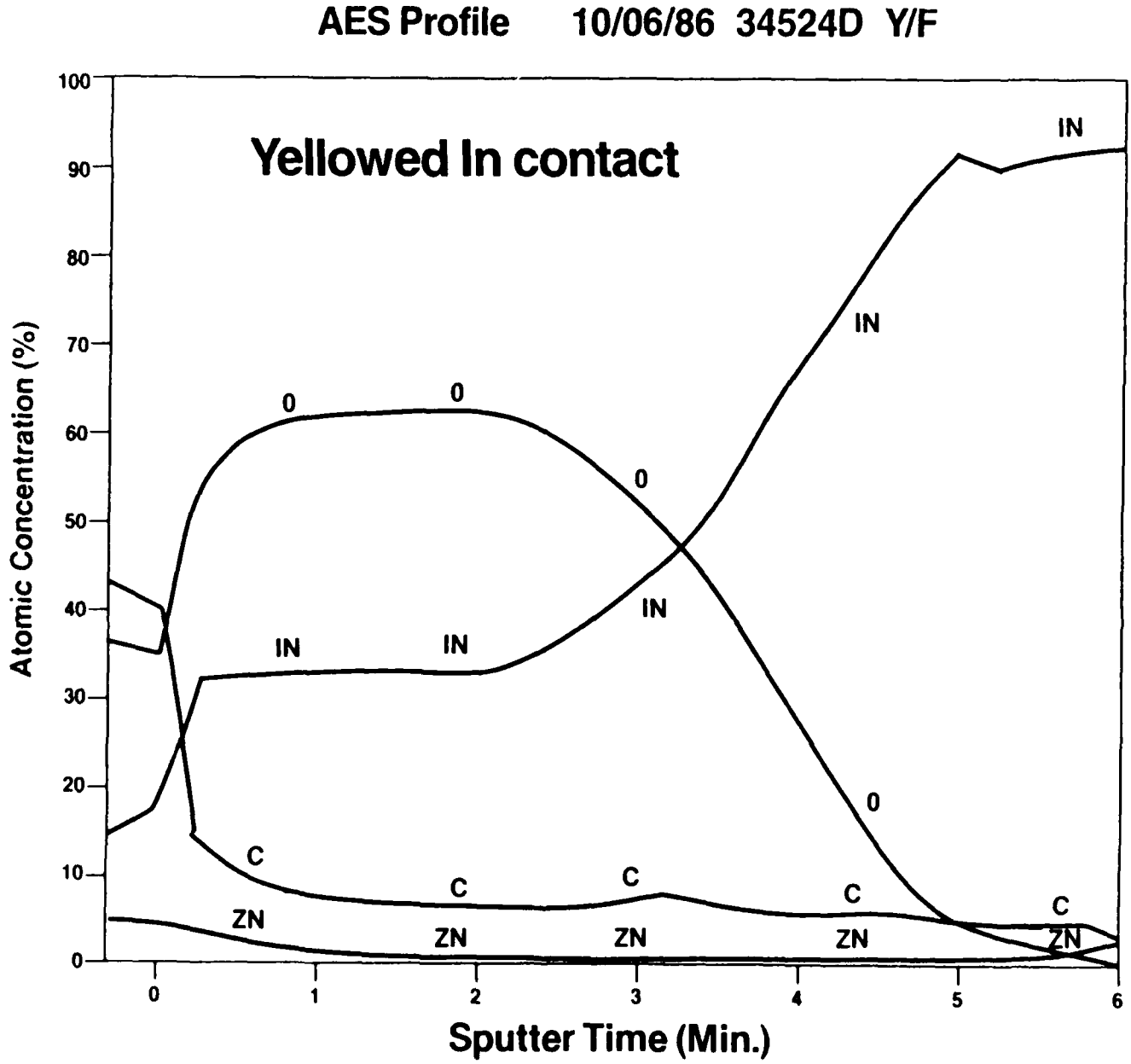

Figure 2-31. Auger Depth Profile of A Yellowed Indium Contact. (Sputtering rate is about 30Å/minute).

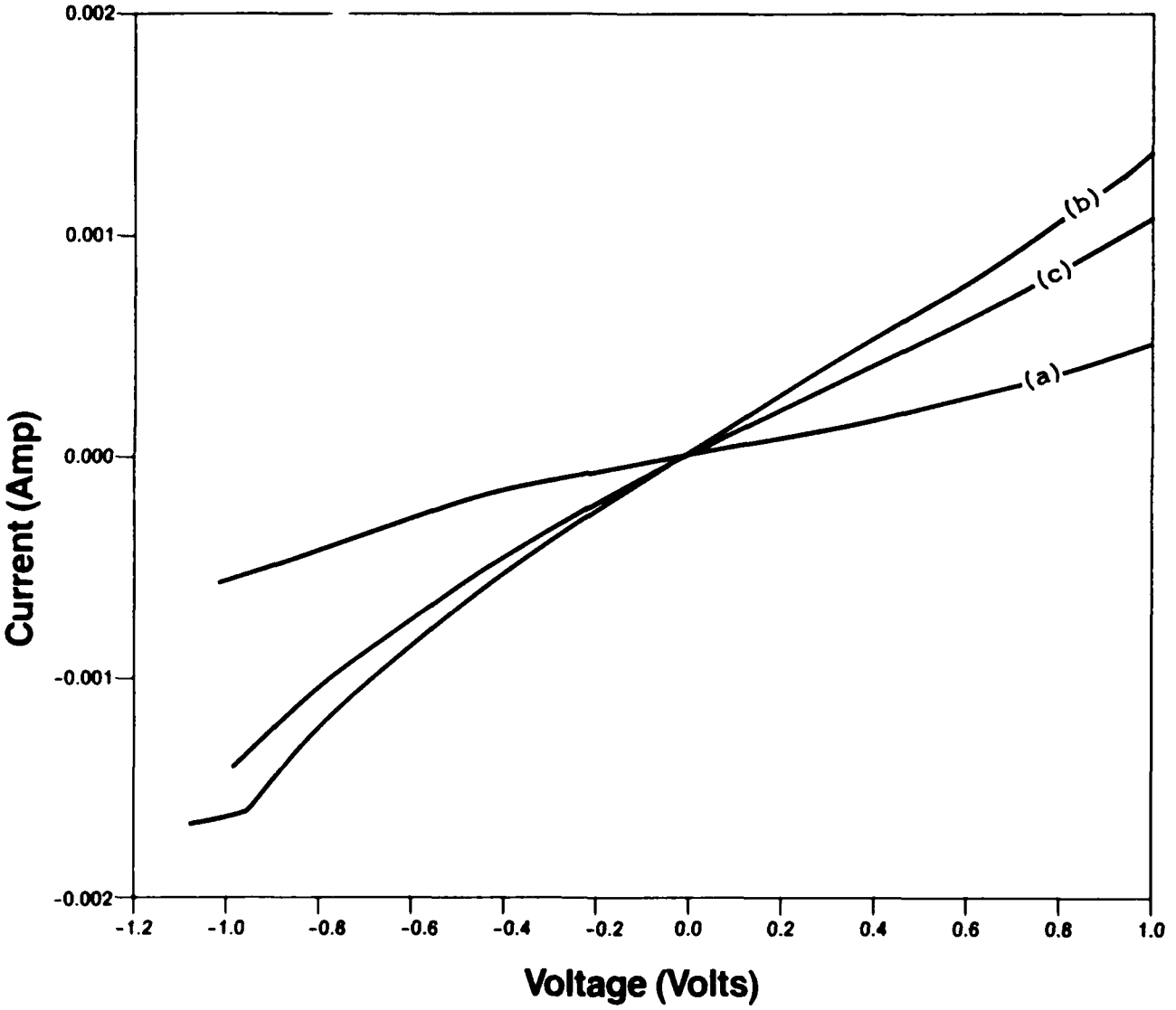

Figure 2-32. Current-Voltage Characteristics Of Al/In/ZnSe/S.I.-GaAS (Co-Planar Electrode Geometry) As A Foundation Of Annealing Time: (a) 5 Minutes, (b) 10 Minutes, (c) 15 Minutes.

3.0 REFERENCES

1. R. Merlin, C. Colvard, M.V. Klein, H. Morkoc, A.Y. Cho, and A.C. Gossard, Appl. Phys. Lett. 36, 43 (1980); A.K. Sood, J. Menendez, M. Cardona, and K. Ploog, Phys. Rev. Lett. 54, 2115 (1985).

2. P.J. Dean, D.C. Herbert, C.J. Werkhoven, B.J. Fitzpatrick and R.N. Bhargava, Phys. Rev. B23, 4888 (1981).

3. J.L. Merz, H. Kukimoto, K. Nassau and J.W. Shiever, Phys. Rev. B6, 545 (1972).

4. P.J. Dean, A.J. Pitt, P.J. Wright, M.L. Young and B. Cockayne, Physica 116B, 508 (1983).

5. P. Blanconnier, J.F. Hogrel, A.M. Jean-Louis, and B. Sermage, J. Appl. Phys. 52, 6895 (1981).

6. C.T. Sah and V.G.K. Reddi, IEEE Trans. El. Dev. ED-11 (1964).

7. E. Schibli and A.G. Milnes, Sol. St. El. 11 (1968) 323.

8. A.K. Jonscher, C. Pickup and S.H. Laid: Semicond. Sci. Technology 1 (1986) 71.

9. Kiyoshi Yoneda, Yuji Hishida, Tadao Toda, Hiroaki Ishit, and Taksuhiko Niina Appl. Phys. Lett. 45 (12), 15 December 1984, P.1300-1302.

10. R.M. Park and H.A. Mar, "Growth and photoluminescence characterization of ZnSe layers grown on (100) Ge by molecular beam epitaxy", J. Materials Research, 1, 543 (1986).

11. H.E. Ruda, "The Application of Free Carrier Absorption to N-ZnSe Materials Characterization", submitted to J. Appl. Phys.

12. H.E. Ruda, J. Appl. Phys. 59, 1220 (1986).

13. H.E. Ruda, J. Appl. Phys. 59, 3516 (1986).

14. R.K. Swank, M. Avan, and J.Z. Devine, J. Appl. Phys. 40, 89 (1969).

END

2-87

DTIC